Title	A hybrid versatile method for state estimation and feature extraction from the trajectory of animal behavior
Author(s)	山﨑, 修平
Citation	大阪大学, 2019, 博士論文
Version Type	VoR
URL	https://doi.org/10.18910/73519
rights	
Note	

Doctoral Thesis

A hybrid versatile method for state estimation and feature extraction from the trajectory of animal behavior

Shuhei Yamazaki

Department of Biological Sciences

Graduate School of Science

Osaka University

July 2019

Contents

GENERAL INTRODUCTION

The primary aim of this research was to develop a method for analyzing the trajectory of animals regardless of the animal species and spatiotemporal scale. For this purpose, I collaborated with Associate Professor Takuya Maekawa of the Graduate School of Information Science and classified animals' trajectory into multiple behavioral states using machine learning, and comprehensively and objectively analyzed the differences in behavioral states. I named this approach as the *st*ate *e*stimation and *f*eature ex*tr*action (STEFTR) method.

Quantitative analysis of animal behavior

In order to analyze animal behavior and investigate its underlying mechanism, it is necessary to record the trajectory, calculate behavioral features, and quantitatively evaluate it. Quantitative analysis of an organism's behavior was pioneered by Howard Berg. Berg and his colleagues recorded the response of *Escherichia coli* to amino acid gradients and revealed that changes in frequency of directional change, "tumbling," depend on a change in concentration of amino acids in a solution, referred to as the biased random walk mechanism (Berg & Brown, 1972; Block et al, 1982). Quantitative analysis of animal (i.e., a multicellular organism with nervous system) behavior was then initiated by Shawn Lockery and colleagues in studies of the nematode, *Caenorhabditis elegans*. In the chemotaxis of *C. elegans,* its trajectory can be classified into a straight movement (run) or frequent directional change (pirouette); these two behavioral states transition stochastically, demonstrating that the biased random walk strategy is also used in animals (Pierce-Shimomura et al., 1999; Lockery, 2011). In wild animals, Lévy

flight, random walk with a power-law tail, has been reported in multiple species (Viswanathan et al, 1996; Viswanathan et al, 2008)

Although quantitative classification of behavior has been achieved, these methods have the following problems: (1) because the classifications are calculated using a different algorithm for each animal species, it is not possible for methods to be used in other animals; (2) they require information regarding posture from high-resolution images and are not suitable for analysis of coarse GPS positional information; and (3) numerous data require manual labelling by humans. Even if the trajectory can be classified, there is still a problem that the extraction of features from the classified behavior state is performed only with subjectively selected parameters. Therefore, I established STEFTR to estimate behavioral states only from the trajectory in an unsupervised manner and to comprehensively analyze and extract behavioral features.

Behavior analysis using the nematode, *C. elegans*

In order to evaluate the newly developed method, it is necessary to analyze the behavior of animals with the following conditions: (1) it is possible to verify the behavioral state from different methods of calculation that classify the behavioral state (i.e., have "correct" labels); (2) the extracted behavioral state can be confirmed by neural activity; (3) the trajectory is recorded under a controlled environment, in which animals receive a controlled stimulus; and (4) the data are less noisy, for example, the measurement time is the same and missing values are not included.

For these reasons, animals in an experimental setting can be considered as proof of principle. Among numerous behaviors, the odor avoidance behavior of *C. elegans* is ideal because detailed quantitative analysis of this behavior has been previously conducted (Kimura et al, 2010; Yamazoe-Umemoto et al, 2015).

In *C. elegans*, in addition to electrophysiology, the recording of neural activity can be achieved using calcium imaging. Tanimoto et al. developed a microscope system that performs calcium imaging under an odor gradient that mimics the stimulus provided during odor avoidance behavior (Tanimoto et al, 2017). Thus, it is considered that the evaluation of the method can be performed using *C. elegans*.

In addition, *C. elegans* has a limited number of neurons (302) and its connectome has been clarified. Moreover, further analysis using genetic and optophysiological techniques can be easily performed. Recently, whole-brain imaging has become available (Nguyen et al., 2016; Venkatachalam et al., 2016). Owing to these characteristics, it appeared relatively simple to analyze the correspondence between neural activities and behavioral features identified using STEFTR.

Aim and approaches of this study

The primary aim of my study was the development of the method to analyze the trajectory in any animal for any spatiotemporal scale. To achieve this goal, I decided to analyze trajectory using only two-dimensional xy coordinates. When considering only xy coordinates, analysis can be performed regardless of the scale of movement and the method of recording,

e.g., a camera or GPS. Furthermore, I used an EM algorithm that does not depend on the initial value for clustering and can perform clustering relatively stably for any distribution. I then comprehensively calculated the characteristics of the behavior and used the obtained information to detect differences between two conditions (e.g., the difference before and after learning).

In order to evaluate whether the developed method was accurate, I analyzed odor avoidance behavior in the nematode *C. elegans.* I confirmed that the behavioral states obtained by clustering were consistent with previous findings and also found the change in neural activity that occurs using calcium imaging under a virtual odor gradient, corresponding to the behavioral features found using STEFTR. In addition, mutants were analyzed, and it was confirmed that groups of features extracted from groups of genes were similar.

Furthermore, in wild animals, we analyzed the behavior of the Adélie penguin, for which previous findings regarding the estimation of behavioral states using multiple sensors were available and confirmed that clustering obtained using STEFTR showed results similar to those reported previously. For the analysis of different scales of behavior, I analyzed seabirds moving over 1000 km and separated the behavioral state of rats as an example in laboratory animals. Moreover, I analyzed the behavior of fruit flies and bats, and revealed that STEFTR was able to extract behavioral features, some of which were consistent with past reports and others were novel findings.

SUMMARY

Animal behavior is the final and integrated output of brain activity. Thus, recording and analyzing behavior is critical to understand the underlying brain function. While recording animal behavior has become easier than ever with the development of compact and inexpensive devices, detailed behavioral data analysis requires sufficient previous knowledge and/or high content data such as video images of animal postures, which makes it difficult for most of the animal behavioral data to be efficiently analyzed to understand brain function. Here, I report a versatile method using a hybrid supervised/unsupervised machine learning approach to efficiently estimate behavioral states and to extract important behavioral features only from low-content animal trajectory data. As proof of principle experiments, I analyzed trajectory data of worms, fruit flies, rats, and bats in the laboratories, and penguins and flying seabirds in the wild, which were recorded with various methods and span a wide range of spatiotemporal scales—from mm to 1000 km in space and from sub-seconds to days in time. I estimated several states during behavior and comprehensively extracted characteristic features from a behavioral state and/or a specific experimental condition. Physiological and genetic experiments in worms revealed that the extracted behavioral features reflected specific neural or gene activities. Thus, our method provides a versatile and unbiased way to extract behavioral features from simple trajectory data to understand brain function.

INTRODUCTION

The brain receives, integrates, and processes a range of ever-changing environmental information to produce relevant behavioral outputs. Therefore, understanding salient behavioral features can augment our understanding of important aspects of environmental information as well as of brain activity, which links the environmental information to behavior. Recent technological development of compact and inexpensive cameras and/or global positioning system (GPS) devices has facilitated convenient monitoring and recording of animal behavior (Brown and de Bivort, 2018; Dell et al., 2014; Egnor and Branson, 2016). However, the behavioral data generated through these approaches are frequently represented as a few simple measures, such as velocity, migratory distance, or the probability of reaching a particular goal, due to the challenges related to identification of specific aspects of behavior to be analyzed; in other words, it is still difficult to figure out how we can describe an animal behavior meaningfully (Berman, 2018). Owing to poor description of behavior, dynamic neural activity, for example, is not sufficiently interpreted even though simultaneous optical monitoring can measure a large number of time-series neural activities (Alivisatos et al., 2012; Landhuis, 2017). This large asymmetry in data richness between neural activity and behavior has emerged as one of the most significant issues in modern neuroscience (Anderson and Perona, 2014; Gomez-Marin et al., 2014; Krakauer et al., 2017).

One way to overcome the challenges in the appropriate descriptions of behavior is to describe its salient features via comprehensive analysis through an approach such as machine

learning. Machine learning involves extracting latent patterns and uncovering knowledge from a

large amount of data (Bishop, 2006). In fact, multiple behavioral analysis methods based on

machine learning have been reported in the last decade (Baek et al., 2002; Branson et al., 2009;

Brown et al., 2013; Dankert et al., 2009; Kabra et al., 2013; Mathis et al., 2018; Robie et al.,

2017; Stephens et al., 2008; Vogelstein et al., 2014; Wiltschko et al., 2015). Most of these

studies have classified behavioral states based on detailed analyses of animal postures as

observed in video images (Dell et al., 2014); the classification of behavioral states into classes,

such as foraging, sleeping, chasing, or fighting, is considered to be critical for efficient

behavioral analysis, as each of the behavioral feature varies differently across different

behavioral states (Egnor and Branson, 2016; Jonsen et al., 2013; Patterson et al., 2008).

Although these methods have worked successfully for the analysis of behavioral videos of

worms, fruit flies, and rodents in laboratories, they have some limitations. First, these methods

are not suitable for analyzing relatively long-distance navigation given their requirement of

recording reasonably large and detailed images of animals in the video frame. Second, the

extraction of behavioral features from a state, as opposed to just state classification, is more

critical in understanding how environmental information and/or brain activities trigger

transitions among states for behavioral response.

To analyze relatively long-distance navigation behavior comprehensively, I

developed a method for the estimation of behavioral states and extraction of relevant behavioral

features based only on the trajectories of animals. For estimating behavioral states, I used an

unsupervised learning method involving the expectation maximization (EM) algorithm

(Dempster et al., 1977) because it is difficult for the human eye to classify behavior into distinct

states without using posture images. For extracting salient behavioral features, I used

information gain, an index used for a supervised learning method (the decision tree analysis)

(Quinlan, 1986), and compared the features between two different experimental conditions (e.g.,

with or without certain stimulus). It is because supervised learning is considered advantageous

in the extraction of characteristic behavioral features and comparing them among multiple

conditions. I named this hybrid supervised/unsupervised machine learning approach as the *st*ate

*e*stimation and *f*eature ex*tr*action (STEFTR) method (Fig. 1).

Because the STEFTR method only uses trajectory information for the analysis, it

becomes possible to analyze the movement behavior of various animals regardless of the

spatiotemporal scale of movement. As proof-of-principle experiments, I analyzed the

trajectories of worms, flies, rats, and bats in laboratories and those of penguins and flying

seabirds in the wild; these experiments involved a spatiotemporal scale ranging from mm to

1000 km in space and from sub-seconds to days in time. The behavioral states of worms and

penguins estimated by the STEFTR method were in reasonable conformation with the ones

described in previous literature, supporting the reliability of our method. I further extracted

learning-dependent behavioral features from a behavioral state of worms, in which one of the

behavioral features is correlated with learning-dependent changes in neural activities. I also

analyzed the behavioral features of mutant strains of worms and found that the patterns of

features are correlated with gene function, suggesting that comprehensive feature extraction

may enable us to estimate unknown functions of a gene product. I was also able to extract

learning-dependent features from bats and pheromone-dependent features from fruit flies. Taken

together, our findings indicate that the STEFTR method allows us to estimate internal state,

neural activity, and gene function related to animal behavior only from movement trajectories,

regardless of the recording method or the spatiotemporal scales.

RESULTS

Estimation of behavioral states

As the first part of the analysis, I classified the trajectory into several behavioral states based on the distribution of a basic behavioral feature. The behavior of animals consists of several states (Jonsen et al., 2013; Patterson et al., 2008), where basic behavioral features such as speed and direction change are likely distributed probabilistically with a center value that is optimal for each state. Thus, behavior can be more easily characterized when the behavioral features are analyzed for each state rather than for the entire behavior as a whole. In fact, classifying the trajectory into several states is one of the essential preprocessing steps in trajectory mining of people and vehicles in data science (Zheng, 2015).

For the state classification, I calculated the averages (Ave) and variances (Var) of four basic behavioral features: velocity (V), temporal changes in velocity (i.e. acceleration, dV), bearing (B), and temporal changes in bearing (dB). These 8 features were represented in the form of histograms. Based on the hypothesis that values of basic behavioral features are likely distributed probabilistically in each state, I considered that histogram peaks may correspond to different behavioral states. One histogram was then regarded as a mixture of Gaussian distributions, and EM algorithm, an iterative method to estimate model parameters that maximize the likelihood of the model (Dempster et al., 1977), was used to estimate the average and variance values of each cluster. The separations of clusters in a histogram were evaluated by the separation index (see Materials and Methods), and the best-separated histogram was

chosen for further analysis. The individual clusters in the histogram were considered to

correspond to different behavioral states. As proof-of-principle experiments, I analyzed the

trajectories of worms and penguins, whose behavioral states have been studied previously using

other methods (Pierce-Shimomura et al., 1999; Yoda et al., 2001).

The roundworm *Caenorhabditis elegans* has been used as a model animal for

quantitative behavioral analysis owing to the ease of tracking behavior (movement for a few cm

on agar surface can be easily recorded with an inexpensive high-resolution camera), optical

monitoring neural activities, and genetic analyses and manipulations (De Bono and Maricq,

2005). Further, the neuronal wiring in *C. elegans* has been described in complete detail (White

et al., 1986). In this study, I focused on the avoidance behavior to the repulsive odor of 2-

nonanone (Fig. 2A, left) (Bargmann et al., 1993; Kimura et al., 2010). I chose this behavioral

paradigm for the proof-of-principle experiment because the odor avoidance behavior has been

quantitatively, although not fully, analyzed previously (Kimura et al., 2010; Yamazoe-

Umemoto et al., 2015). The behavior of the worms was recorded with a USB camera for 12

minutes, and the position of each worm's centroid was extracted every second (Table 1).

I calculated the separation index in 8 basic features, and the variance values for

bearing change with 5 clusters turned out to be the best (*dB_Var*, Fig. 2B and C). Upon

mapping the clusters on to the trajectories, I found that cluster 0 corresponds to relatively

straight part, while the other clusters correspond to more complex parts (Fig. 2D, upper panel).

Cluster 0 and clusters 1-4 mainly corresponded to "run" and "pirouette," respectively, which are the classic two behavioral states of worms and have been found in multiple types of sensory behavior (Fig. 2D, lower panel) (Lockery, 2011; Pierce-Shimomura et al., 1999). "Run" constitutes a relatively straight movement, while "pirouette" is characterized by short, straight movement divided by frequent large changes in angle (turns and reversals). Runs and pirouettes are usually classified based on a threshold value for the duration between consecutive large angle changes (Pierce-Shimomura et al., 1999), unlike in this method. I collectively regarded clusters 1-4 as "cluster 1" because the positional information of worms does not appropriately reflect their actual locations during pirouettes due to insufficient spatiotemporal resolution of the recording system for relatively long-distance navigation, such as odor avoidance behavior (Yamazoe-Umemoto et al., 2015). I found that more than 90% of the cluster 0 and 1 corresponded with the run and pirouette, respectively (Fig. 2E, F and Suppl. Fig. 1A). Therefore, I concluded that the STEFTR method properly classified the odor avoidance behavior into distinct behavioral states. Although some cluster(s) do not appear to be Gaussian distributed (Fig. 2C), the high matching rate supports the legitimacy of this method (see also the following sections for penguins).

Next, I applied the same process to the trajectories of penguins obtained using GPS devices. Penguins are good model wild animals for studying long-distance navigation given their relatively large body size and their habit of returning to a colony, which make the attachment and the recovery of GPS data easy (Yoda, 2018; Yoda et al., 2001). In this study,

GPS and depth sensors were attached to 11 penguins from a colony in the Antarctic Continent; the depth sensors were used to evaluate the accuracy of state estimation (see below). The penguins moved by walking and swimming about 10 km for feeding, and each dataset contained up to 2 days of data recordings (Table 1 and Fig. 3A). Like in the case of worms, 8 basic behavioral features were extracted from the penguin trajectory data and represented as histograms. I chose the average velocity (V_Ave) as it showed the highest separation index (Fig. 3B). The EM algorithm classified it into 5 clusters (Fig. 3C, D and E upper panel).

Interestingly, the clusters exhibited significantly different distributions in multiple behavioral features. For example, the values for the duration of each bout were much longer in cluster 0 than in clusters 1, 2, and 3 (Fig. 3E, middle panel). In addition, although the clusters were classified only based on the horizontal velocities, the depths for cluster 0 and 1 were significantly closer to zero than those for clusters 2, 3, and 4 (Fig. 3E, lower panel). These results are consistent with the idea that each cluster reflects a behavioral state that is a complex function of multiple behavioral features.

To evaluate whether the clusters actually reflect different behavioral states, I compare the results with the typical manual classification into four states (resting, transit by walking, transit by swimming, and diving), based on diving depth (from depth sensor), movement velocity, and distance from the colony (both calculated from the GPS positional information) (Watanabe et al., 2012; Yoda et al., 2001). Penguins stayed and rested at the

colony (location does not change much; depth is zero), moved on land and ice mainly by

walking (location changes relatively slowly; depth is near-zero), swim in the sea to go to the

foraging area (location changes quickly; depth is relatively shallow in general and sometimes

increases when they are moving towards the feeding area), dive deeply at the foraging area

(location does not change much; dives occur continuously in bouts), and then come back to the

colony by swimming and walking. The resting at the colony and swimming correlated with

clusters 0 and 4, respectively (Fig. 3F, G and Suppl. Fig. 2A). In addition, most of clusters 1 and

2 correlated with walking, while about 50% of cluster 3 corresponded to diving (Fig. 3G and

Suppl. Fig. 2A). Thus, when a behavioral state is classified to a cluster other than cluster 3, the

penguin is likely to be resting, walking, or swimming. If a behavioral state is classified to

cluster 3, which is ~10% of all the behavior recorded, the penguin is either diving or swimming.

Remarkably, although the clustering is only based on the trajectories of 11 penguins for a few

days, the false positive rates were less than 10% and the sensitivity of the analysis was greater

than 90% in all the cases (Fig. 3H). Thus, I concluded that the STEFTR method can reasonably

estimate different behavioral states only based on trajectory data.

In order to verify the evaluation process by the separation index, I compared the

results of the state estimation with the 1st and 2nd best-separated histograms for the worms and

the penguins (indicated by red and yellow rectangles, respectively, in Fig. 2B and 3B). In both

animal species, the estimated behavioral states based on the 2nd best separation index exhibited

a similar tendency to those of the best separation index, although the correlations between

clusters and behavioral states were less clear (Suppl. Fig. 1B-E and 2B-D). These results

strongly support the selection of the basic behavioral feature by the separation index.

The STEFTR method was also applied to the trajectories of flying seabirds in the

wild and rats in the laboratory. The seabirds, *Calonectris leucomelas*, traveled ~100 times

longer distances (up to 1,000 km) with ~10 times the speeds compared to penguins (Matsumoto

et al., 2017; Yoda et al., 2014). For the animals, the variance of bearing (*B_Var*) with 4 clusters

were chosen (Fig. 4A-C). In the case of rats, the variance of velocity change (*dV_Var*) with 4

clusters was chosen (Fig. 4D-G). In both animal species, significant differences among clusters

were observed in duration and directedness, for example (Fig. 4D and H). Such information can

help ecologists estimate the candidates for feeding areas where fishes may be more densely

distributed and discover biologically important marine areas. It can also help neuroscientists in

estimating candidate conditions to further explore specific neural activities.

Comprehensive extraction of behavioral features modulated by learning

As a second part of the STEFTR method, comprehensive feature extraction was

performed by comparing a specific behavioral state in two different conditions, such as cluster 0

of worms before and after learning. Comprehensive semi-automated analysis can be very

helpful to compare behavioral features in two conditions. This is because even when the overall

result of behavioral responses is different in two conditions, it is still difficult to quantitatively

determine which part of the trajectories are different (Fig. 2A left and right, for example).

Furthermore, even if several behavioral features are found to be different, it is possible that other more prominent feature differences may exist. I considered that learning-dependent changes in behavior should be one of the best models for comprehensive feature extraction because the differences in behavioral features should reflect learning-dependent changes in neural/brain activities.

As a useful index for feature extraction, I chose information gain, the index for decision tree analysis (Quinlan, 1986). Binary decision tree analysis is for splitting a dataset into two sub-groups by automatically selecting the best feature and its parameter showing the largest information gain (i.e., difference of uncertainty, or "information entropy", between before and after division). Each data point is then classified into one of the sub-classes based on whether it has a larger or smaller value than an automatically determined threshold. When applied for binary classification, decision tree analysis automatically evaluates the classification performance of a large number of features as designed by the researchers. This analysis results in the extraction of certain features, allowing us to easily understand the utility of particular features in the classification. This approach is substantially different from those that employ support vector machines and/or deep neural networks, wherein the relationships between the classification and the features of the data cannot be easily discerned.

I first analyzed learning-dependent changes in worm odor avoidance behavior. Worm odor avoidance behavior is enhanced by pre-exposure to the odor as a type of non-associative

learning, and pre-exposed worms migrate significantly longer distances from the odor source

than control worms do during the same period (Fig. 2A) (Kimura et al., 2010). This

phenomenon is interesting because prior exposure to a stimulus generally causes a reduction,

instead of enhancement, of the response to the stimulus through adaptation or habituation.

Although this is a simple form of learning, this odor learning is modulated by multiple

neuromodulators, including dopamine, octopamine (the worm counterpart of mammalian

noradrenaline), and neuropeptides (Kimura et al., 2010; Yamazoe-Umemoto et al., 2015).

Previous quantitative analyses have shown that the enhanced odor avoidance behavior is not

caused by changes in speed, but mostly by increases in run duration (Yamazoe-Umemoto et al.,

2015). However, this did not rule out the possibility that other behavioral features play more

profound effects.

As an example of comprehensive feature extraction from a behavioral state, I focused

on learning-dependent changes in cluster 0 (run) because the values of their centroid migration

are quantitatively more reliable than cluster 1 (pirouette) as mentioned above. In addition to the

basic behavioral features used for the estimation of behavioral states (V, dV, B, and dB), I also

calculated directedness (Dir) (Gorelik and Gautreau, 2014), and the odor concentration (C) and

temporal change in odor concentration (dC) that each worm experienced during the odor

avoidance behavior; C and dC were calculated based on actual measurements of the dynamic

odor gradient (Tanimoto et al., 2017; Yamazoe-Umemoto et al., 2018). For these, I calculated

the initiation (Ini), middle (Mid), termination (Ter), and all (All) values of a cluster 0 segment

(Fig. 5A). In addition, different time windows (1-6 s in this case) were used to calculate these values because a behavioral feature could be apparent only within a specific temporal window (for example, velocity of run (i.e. cluster 0) starts decreasing 2 s before the end of a run (Pierce-Shimomura et al., 1999)). I also calculated durations (*Dur*) of cluster 0 and 1, and the weathervane index (*WV*) (Iino and Yoshida, 2009). Information gain for each of these features was compared between naive/mock and pre-exposed conditions (Fig. 5B, for example). The information gain values for each of the features have been summarized in Table 2, and the details are described in Supplementary Tables 2-11.

Through this analysis, I was able to find new as well as previously known behavioral features that exhibited learning-dependent changes. First, I found that the duration of each cluster 0 (*Clst0Dur*) exhibited higher information gain (Table 2), which corresponded to significantly increased cluster 0 duration (Fig. 6B). This result is consistent with the findings from previous reports (Kimura et al., 2010; Yamazoe-Umemoto et al., 2015), highlighting the reliability of this method. I also found that the velocity at the beginning of each cluster 0 (*V_Ini*) consistently exhibited higher information gain in the average and median values in multiple time windows (Table 2); these values were also significantly different in the pre-exposed worms as compared to the control worms (Fig. 6C). The previous study has not identified this difference as only average values per run (*i.e.* cluster 0) have been calculated in the study (Yamazoe-Umemoto et al., 2015). Although the contribution of this behavioral feature to enhanced odor avoidance is unclear at present, our results indicate that the STEFTR method can

reveal characteristic feature(s) under specific conditions, which is difficult for human analyses to accomplish.

Odor stimuli during runs, which likely drive the worms' odor avoidance behavior, were also found to be consistently modulated (Table 2). In fact, odor concentration (C) was significantly lower, and the temporal change in odor concentration (dC) was significantly closer to zero (i.e. shallower) in a learning-dependent manner (Fig. 6D and E). Because the previous study demonstrated that worm odor avoidance behavior depends on dC rather than C at least in the naive condition (Tanimoto et al., 2017), one possibility is that the changes in the responsiveness of worms to dC was the underlying reason for the enhanced odor avoidance. However, it is also possible that the odor-experienced worms were somehow located farther away from the odor source than the unexperienced worms, and hence, sensed lower odor concentrations and shallower odor concentration change than the latter.

Responsiveness of sensory neurons to odor increase was modulated by the odor learning

(This experiment was performed by Yosuke Ikejiri.)

If the change in sensitivity to dC/dt is the reason underlying enhanced odor avoidance behavior, it should be associated with changes in neural activity. Thus, I analyzed the responsiveness of a likely candidate, ASH nociceptive neurons (Bargmann, 2006; Kaplan, 1996). Previously, we have established the OSB2 microscope system that allows for *in vivo* calcium imaging of *C. elegans* neurons in the presence of odor stimuli resembling those that the

worms experience during the odor avoidance behavior in the plates (Fig. 7A) (Tanimoto et al., 2017). Using the OSB2 system, we found that ASH neurons are the major sensory neurons to cause pirouettes upon increases in 2-nonanone concentration (Tanimoto et al., 2017). However, whether the ASH response is modulated by 2-nonanone experience has not yet been studied.

We found that ASH responses were indeed modulated by prior odor experience. When the worms were stimulated with a 5 nM/s odor increase rate, which is the lowest rate of change to cause the threshold-level behavioral response in the previous study (Tanimoto et al., 2017), ASH neurons in naive as well as mock-treated worms exhibited robust responses (Fig. 7B). However, the ASH responses were significantly reduced in the pre-exposed worms (Fig. 7B and C). This suggests that prior odor experience causes a reduction in the neuronal response to a slight increase in odor concentration, subsequently causing longer run durations and enhanced odor avoidance behavior (Fig. 7D).

Extracted behavioral features of mutant strains correspond to gene function

Next, I comprehensively analyzed learning-dependent behavioral changes in the mutant *C. elegans* strains. Many mutant strains of *C. elegans* showing impaired learning have already been isolated and characterized (Bargmann, 2006; Sasakura and Mori, 2013), and the behavioral abnormalities observed in these mutants should reflect the role of the causal genes in neural function. In fact, Yamazoe-Umemoto et al. have previously shown that two different groups of genes involved in the enhanced odor avoidance behavior cause different abnormalities

in behavioral features when mutated (Yamazoe-Umemoto et al., 2015). However, as the behavioral features exhibited by a mutant strain could be different from one another, identification of abnormal behavioral features is often laborious and time-consuming.

In addition to studying the previously described mutants with defective enhanced odor avoidance behavior (*egl-3* and *egl-21* for neuropeptide biosynthesis, and *dop-3* for dopamine receptor) (Kass et al., 2001; Suo et al., 2004; Yamazoe-Umemoto et al., 2015), I also analyzed mutant strains found to be involved in the phenomenon in this study (*ocr-2* and *osm-9* for TRP channels; *tax-4* for CNG channel; *eat-4* for vesicular glutamate transporter; *pkc-1* for protein kinase) (Colbert et al., 1997; Komatsu et al., 1996; Land et al., 1994; Lee et al., 1999; Tobin et al., 2002) (Table 3).

Neuropeptide mutant strains did not exhibit learning-dependent changes in behavioral features, except for the velocity of *egl-3(ok979)*. This result is consistent with the previous finding that neuropeptide signaling is required for the acquisition of odor memory (Yamazoe-Umemoto et al., 2015). *egl-3(ok979)* may have exhibited stronger phenotypes than *egl-3(n589)* because they are nonsense and missense mutants, respectively. Also consistent with the previous report (Yamazoe-Umemoto et al., 2015), the *dop-3* mutants exhibited abnormalities in direction-related behavioral features (*B* and *Dir*) while the changes in cluster 0 durations and velocities are similar to those of wild-type worms (Table 3). Furthermore, with respect to the newly added mutant strain, similar patterns are observed in *ocr-2* and *osm-9* mutants of the TRP channel involved in sensory perception. On the other hand, *tax-4*, which is

also involved in sensory perception but expressed in a different set of sensory neurons (Komatsu et al., 1996; Tobin et al., 2002), and *eat-4* and *pkc-1* mutants showed different patterns of abnormalities. Taken together, our results suggest that the patterns of features extracted from mutant strains may reflect functional groupings of the mutated genes. Thus, profiling and classification of extracted mutant features of unknown genes may be useful in the estimation of their physiological functions.

Feature extraction of fly sexual behavior

Next, I applied the technique to comprehensive feature extraction of animal behavior under specific situations in two different conditions—heterosexual chasing behavior of *Drosophila melanogaster* with or without pheromone sensation. On an experimental tracking system (Fig. 8A), male flies chased the target female flies' abdomens after tapping them with their forelegs to sense the cuticular pheromone, although males do not show such chasing behavior before tapping (Kohatsu et al., 2011). While this pheromone-driven behavior has been generally used for the observation of neural activity during courtship behavior in fruit flies, the behavioral features have not yet been elucidated comprehensively.

In this study, I used a tracking system as described in previous studies, where a male was exhibited the moving female abdomen with 8 times left-right round trip after a pheromone sensation (Fig. 8A) (Kohatsu et al., 2011). I detected positive information gains in the velocity, changes in velocity, bearing, and changes in bearing in a pheromone sensation-dependent

manner (Fig. 8B). Unexpectedly, the information gains of velocity were higher in the earlier

round trips and decreased over the trips (Fig. 8B). This suggests that the pheromonal effect

promoting chasing behavior decreases over time. To confirm the result of the STEFTR method,

I re-analyzed the speed of the male locomotion along with time-series. Consistent with the

STEFTR result, the velocity of males that had tapped the female significantly decreased over

the trips (orange group in Fig. 8C; significant differences between rounds 1, 4, and 8), whereas

that of control flies (gray group in Fig. 8C) remained mostly unchanged (significant difference

only between rounds 1 and 5). Thus, the STEFTR method can even uncover behavioral features

that fluctuate over time. The decreased tracking velocity may reflect a decrease in motivation in

the fly brain, which can be assessed directly by observing the temporal changes in neuronal

activity related to the courtship-motivation circuit in the fly brain (Yamamoto and Koganezawa,

2013; Zhang et al., 2018).

Feature extraction of learning-dependent modulation of acoustic navigation in bats

To further demonstrate the general applicability of the method, I examined features

of acoustic navigation in bats. Yamada has previously reported that bats improve their flight

trajectory in an indoor space with obstacles in a learning-dependent manner (Yamada 2017).

Here, I optimized features such as velocity (V), distance to the obstacle chain array (R_obs and

R_x), and horizontal bearing of the flight (B_hori) for the experimental paradigm (Fig. 9A and

B). Interestingly, although the velocity (V) itself was modulated by flight experience, the change

in velocity (dV) was not (Fig. 9C and D), suggesting that bats determine flight speed before

initiating navigation, but not during navigation, at least in this experimental condition. As the

vocalizations of bats reflect their attention or decisions (Moss and Surlykke, 2010), our results

suggest that the STEFTR method can be used to elucidate such higher brain functions during

navigation.

DISCUSSION

Measuring and analyzing behavior is one of the most prominent steps in understanding brain function. In order to utilize "behavioral big data", I developed a hybrid supervised/unsupervised technique, the STEFTR method, to estimate behavioral states and to efficiently extract behavioral features solely from the trajectories of animal movement. The behavioral states of worms and penguins estimated with the STEFTR method were in reasonable agreement with the ones based on previous knowledge, highlighting the validity of our method. In addition, one of the learning-dependent behavioral features extracted from worms corresponded to a change in neural activity. Furthermore, I was able to identify temporally dynamic changes through feature extraction from fly courtship behavioral data.

One of the advantages of the STEFTR method is its versatility. Multiple methods have been reported for the behavioral analysis of specific animals under specific conditions (Baek et al., 2002; Branson et al., 2009; Brown et al., 2013; Dankert et al., 2009; Kabra et al., 2013; Mathis et al., 2018; Robie et al., 2017; Stephens et al., 2008; Vogelstein et al., 2014; Wiltschko et al., 2015). However, the animals and experimental conditions for which each of these methods can be applied are rather limited. For example, it is still not easy to effectively and robustly extract an animal's posture from a video image, especially in the wild. Even in laboratories, the parameters generally need to be adjusted again when imaging conditions changed (Dell et al., 2014; Egnor and Branson, 2016). In contrast to these methods, our method

allows for behavioral analysis based on positional information that can be extracted from animal video images as well as from different methods such as a GPS device.

As a first step of the STEFTR method, I estimated behavioral states from animal trajectories. State estimation is one of the critical processes of movement analysis of animals in the wild as well as of cars and people in ecology and data science, respectively (Egnor and Branson, 2016; Jonsen et al., 2013; Patterson et al., 2008; Zheng, 2015). However, the analytical methods that can be applied to the analysis of various types of animals (and cars and people) are still in debate (Gurarie et al., 2016; Zheng, 2015). In the STEFTR method, I aimed to analyze behavior without previous knowledge of the animal and/or experimental condition and independent of the spatiotemporal scale of the behavior. For this purpose, I analyzed migratory velocity and direction, the most fundamental elements of moving objects, with appropriate moving-averaged data. Because different types of behavioral features are observed in different temporal scales from milliseconds to days or months (Buhusi and Meck, 2005), I assumed that different levels of behavioral states will be extracted with different temporal resolution. I further hypothesized that a proper combination of recording time, time unit, and temporal resolution may determine the type of behavioral state to be extracted. Our results suggest that the ratio among total recording time, time unit, and temporal window used in this study were proper to extract well-known behavioral states in worms and penguins (Fig. 2D-F and 3F-H). Furthermore, when I used ~0.15% temporal window for analysis of worms, the clusters obtained from the analysis did not match to run and pirouette (Suppl. Fig. 1F). This

result also supports the idea that a proper temporal window is required to extract certain

behavioral states. Still, those clusters with 0.15% temporal window may reflect other behavioral

states of worms, which have not been studied yet.

State estimation based only on trajectory analysis using the STEFTR method is not

perfect, as shown in the case of penguins (Fig. 3F-H). However, the estimated behavioral states

likely provide us with important information for further experiments, such as when and where

in the spatiotemporal behavioral profile of the animal behavior should be analyzed in detail,

especially in the case where the behavior has not been studied intensively in a quantitative

manner. For example, relatively small movements at places distant from their nest in the wild

may correspond to the feeding area. For neurobiological/physiological analysis, the transition

from one state to the other could be triggered by a specific change in the sensory stimulus and

associated with specific neural activities. It should also be noted that the STEFTR method

allows semi-automatic state estimation and feature extraction, which is suitable for large-scale

behavioral analysis of mutant strains of laboratory model animals (Table 3).

Estimation of behavioral states (or behavioral modes) based on animal trajectories

have been performed previously by various methods. The Expectation-Maximization binary

Clustering (EMbC) method is the most similar to our method (Garriga et al., 2016). In the

EMbC method, a few behavioral features, such as velocity and turn angle, were classified into

two groups based on higher (H) or lower (L) values compared to a threshold, and the trajectories

were segmented using combinations of the classifications (e.g., HH, HL, LH, or LL for velocity-turn angle). In that study, bat trajectories were analyzed by the EMbC method and compared with the labels by experts. True positive rates (TPR) for roost, forage, and commute were 9%, 94%, and 91%, respectively, which were at least comparable with the TPR of our method for worms and penguins ("sensitivity" in Fig. 2F and 3H). When state estimation from trajectory data with classic methods (first passage time, speed-tortuosity threshold, Hidden Markov Model, etc.) or with machine learning methods (linear discriminant analysis, classification and regression trees, support vector machine, etc.) were systematically compared with ground truth data, TPR of the classic methods were about 30-80%, and 80-90% for machine learning (Bennison et al., 2017; Nathan et al., 2012). Furthermore, even in a study that classified the behavioral state of Drosophila or mice based on high content video data with machine learning analysis, about 4-5% errors were observed (Kabra et al., 2013). This comparison of our method with earlier methods is not accurate as these studies used data different from ours. Still, I consider that our STEFTR method is one of the efficient methods to estimate behavioral states from animal trajectories.

For comprehensive feature extraction, I used information gain, an index used in decision tree analysis. Decision tree analysis is one of the machine learning techniques used for classification. Classification analysis involves classifying new, unlabeled data into appropriate classes using characteristic features and the parameters that have been extracted from the known class-labeled data. In the present study, however, the classification itself was not meaningful

because the data were already classified (with/without learning or with/without sex pheromone). Instead, I focused on the procedure in the classification that identifies features useful for distinguishing between the two classes. In other words, behavioral features that are different between two classes (i.e., conditions) should be able to effectively classify the behavioral data of animals in two conditions. To our knowledge, our STEFTR method is the first pipeline to comprehensively extract behavioral features of a behavioral state in two different conditions.

Although the STEFTR method does not directly provide information about brain/neural activity underlying animal behavior, it provides us with clues required to formulate hypotheses related to the experimental investigation of the neural activity, as shown in the case of learning-dependent changes in behavioral features and neural activity (Fig. 7). For example, animals in the wild experience continuously changing visual, auditory, and olfactory stimuli, each of which contains multi-dimensional information (color, shape, tone, different chemical compounds, etc.). Therefore, it is difficult to identify which aspect(s) of the particular stimulus actually triggers a change in animal behavior. Estimation of behavioral states using the STEFTR method will allow us to identify the behavior-triggering stimulus by focusing on the timing and/or place of the behavioral transition. Similarly, large-scale recording of neural activities from moving animals in the laboratory itself is difficult to interpret. However, state estimation and feature extraction of the behavior will greatly facilitate the identification of neural activities that are associated with behavioral transitions and/or specific behavioral features.

MATERIAL AND METHODS

Overview of behavioral state estimation

For the analysis of trajectory information of an animal obtained from video images or from the GPS device attached to an animal, approximately 1/1,000 and 1/100 of the median recording time across animals were used as a unit for time frame and the time window for moving average, respectively (Table 1). These values were used to draw the 8 histograms of the averages (*Ave*) and the variances (*Var*) of velocity (*V*), bearing (*B*), time-differential of *V* (*dV*) and *B* (*dB*) as the basic behavioral features. The time window for moving average was critical to reduce noise and to detect relatively long trends of behavior (see Discussion). Each histogram was regarded as a mixture of normal distributions, and EM algorithm was used to estimate the number of clusters (i.e. normal distributions) and their boundaries. I then calculated how many individual clusters in a histogram were well-separated using the separation index, and a histogram with the best separation index was chosen for further analysis (for details, see the following sections). The individual clusters in the chosen histogram are considered to be corresponding to different behavioral states. In the case of worms, the EM analysis was performed with specifying the maximum cluster number of 20. In other cases, maximum cluster number 5 was predetermined based on the knowledge that the number of basic behavioral states are several in general (Patterson et al., 2008).

The EM algorithm assigns a cluster label to each time frame although the clustering results should be smooth in time because each cluster should reflect a behavioral state of an

animal. To smooth out the clustering results and removing outlying results, moving average was

again applied to the cluster labels, which resulted in clusters resemble to the human-labeled

behavioral states.

When the value of a basic behavioral feature changes suddenly and largely, the

influence of the change may extend over a wide range. For example, if an animal moving

straightly initiates local search suddenly, *dB* value will be 0°, 0°, 0°, 0°, 0°, 0°, 180°, 0°, 90°, 0°,

270°, etc. If moving average with ±5 time frame is applied, the value change occurs from -5

time frame of the sudden value change, which should be compensated. Because worm's clusters

0 and 1 corresponded to this case, the beginning and the end of each cluster 0 was extended by

the half of time window.

The cluster labels obtained as described above were mapped to the corresponding

trajectory position with colors. I used a custom-made python program for calculating basic

behavioral features, Weka data mining software (the University of Waikato, New Zealand)

(Frank et al., 2016) for EM calculation, and Excel (Microsoft) for others.

EM algorithm for cluster analysis

A set of values of the ith basic behavioral feature $F_i (e.g., \text{V\_Ave})$, which were

extracted from trajectories of interest, and the number of clusters N were given. I employed the

EM algorithm to cluster F_i into N clusters, i.e., a mixture of N Gaussians. The probability

distribution of the Gaussian mixtures M_N is represented as follows:

$$p(f_i|M_N) = \sum_{n=1}^{N} \pi_n N(f_i, \mu_n, \sigma_n),$$

where f_i is one of the feature values among of F_i, π_n is the mixture weight of the nth

Gaussian, μ_n is the mean of the nth Gaussian, and σ_n is the standard deviation of the nth

Gaussian. The EM algorithm was used to estimate the cluster parameters: π_n, μ_n, and σ_n.

Determination of cluster number using log-likelihood for model

To find the best cluster number N, we evaluated a set of clusters obtained by the EM

algorithm using log-likelihood of a set of feature values F_i under model M_n (n shows the

cluster number). That is, (i) we performed the EM algorithm to obtain the cluster parameters for

each n, which increased from 1 by 1. (ii) If the log-likelihood of F_i for M_n was increased

compared with that for M_{n-1}, n was further increased. (iii) If not, the best N was determined as

$n - 1$. The Weka software (Frank et al., 2016) was used for this process.

Automatic selection of basic behavioral feature by separation index

To choose a histogram that best represents multiple behavior states, we calculated the

"separation index" based on the following two criteria: (i) the distances among clusters were

large and (ii) a peak of each cluster was apparent. The first criterion was calculated based on the

overlapping area of different clusters. The second criterion was designed based on an idea that,

when behavior clusters are not separated, the histogram (mixture of the clusters) seems to have

no apparent peaks. Based on the above criteria, the separation index of a histogram was

calculated as follows:

$$s(H) = (1 - \text{Ov}(M_N)) + \frac{\min(N, \text{Mx}(H))}{N},$$

where $\text{Ov}(M_N)$ represents the proportion of overlapping area of adjacent Gaussian

distributions in M_N, and $\text{Mx}(H)$ represents the number of local maxima in the histogram H.

To calculate local maxima, we first estimated the probability density function of H using the

kernel density estimation and then calculated the derivative of the function. Note that, to

eliminate noise local maxima, we ignored local maxima smaller than 0.1%. A histogram with

the largest index was selected for further analysis.

Feature extraction with information gain

       I leverage information gain to evaluate the classification ability of each feature, i.e.,

its ability to identify a characteristic of a state (cluster). Information entropy is used to compute

the ambiguity of a set of data points according to the following formula:

$$H = -\sum_{n=1}^{N} p_n \log_2 p_n,$$

where p_n is the proportion of data points belonging to the nth class (cluster). Given that I

classify all the data points into two groups (i.e. two experimental conditions) using a particular

threshold related to a specific feature, the feature is considered to be a characteristic feature (in

that it classifies the data points well) if the ambiguity within the two groups is lower than that of

the original data set. Thus, I evaluated features in terms of their ability in ambiguity reduction upon classification (information gain).

For worm odor avoidance behavior, I extracted behavioral features that have positive information gain in naive versus pre-exposed worms or in mock-treated versus pre-exposed worms (see below). Next, I chose the extracted features that were common for both comparisons; these features were termed as "features modulated in a learning-dependent manner." For flies, behavioral features were compared between with or without pheromone tapping. For bats, behavioral features were compared between unfamiliar flights (1st-3rd) and familiar (10th-12th) flights. The Weka software was used for these calculations.

Behavioral parameters included in a feature vector

For the machine learning analysis of worm's odor avoidance behavior, the following behavioral features were calculated for each cluster 0 segment from the coordinates of the centroid of the trajectory: velocity (V), bearing (B), odor concentration the worm experienced during the run (C), the time differential values for these (dV, dB, and dC), directedness (Dir) (Gorelik and Gautreau, 2014), curvature (called weathervane; WV) (Iino and Yoshida, 2009), and durations of cluster 0 and 1 (*Clst0Dur* and *Clst1Dur*, respectively). For V, dV, B, dB, C, dC, and Dir, the average (*Ave*) and median (*Med*) values for at the initiation (*Ini*), middle (*Mid*), termination (*Ter*), and all (*All*) periods of a cluster 0 segment were calculated. A total of 333 features was calculated by combining all these features.

For analyzing changes in the flight of bats, the following behavioral features in each flight were calculated from the coordinates of the bats and obstacles: three-dimensional flight velocity (V), horizontal and vertical bearings of the flight (B_hori and B_vert, respectively), distance (R_obs) and bearing (B_obs) of the bat to the nearest edge point of the obstacle chain array, longitudinal directional distance to the frontal chain array (R_x), and lateral directional distance to the inside pitch of the chain array (R_y). Time-differential values were calculated for V (dV), B (dB), dB (ddB), and the flight height (dH), which were calculated with frame units of the high-speed video cameras (1/125 s). All flight trajectories were divided into three segments: early, middle, and late terms. The time window for the analysis of each behavioral feature was 0.1 s, 0.2 s, or 0.3 s before or while ($t = 0$) passing through the chain array. A total of 42 features was calculated by combining all these features.

Excel and Visual C# (Microsoft) were used for the calculations, while the Beeswarm package for R (The R Project) was used to obtain a scatter plot of the data.

Worms *(This experiment was performed by Akiko Yamazoe-Umemoto and Kosuke Fujita)*

The culture and handling of *Caenorhabditis elegans* strains were performed according to techniques described previously (Brenner, 1974). Wild-type Bristol strain RRID:WB-STRAIN:N2_Male and mutant strains RRID:WB-STRAIN:MT1219 *egl-3(n589)*, RRID:WB-STRAIN:VC671 *egl-3(ok979)*, RRID:WB-STRAIN:KP2018 egl-21(n476),

RRID:WB-STRAIN:CX4544 *ocr-2(ak47)*, RRID:WB-STRAIN:JC1636 *osm-9(ky10)*, and

RRID:WB-STRAIN:FK127 *tax-4(p678)*, RRID:WB-STRAIN:MT6308 *eat-4(ky5)*, and

RRID:WB-STRAIN:IK105 *pkc-1(nj1)* were obtained from the Caenorhabditis Genetics Center

at the University of Minnesota, USA. The RRID:WB-STRAIN:KDK1 *dop-3(tm1356)* strain

was originally obtained from the National BioResource Project (Japan) and back-crossed with

the wild-type N2 strain five times.

A 2-nonanone avoidance assay was performed according to the protocol described

previously (Kimura et al., 2010; Yamazoe-Umemoto et al., 2015). Briefly, 2-3 young adult

hermaphrodite worms grown synchronously were placed in the center of a 9-cm nematode

growth media (NGM) plate. Worm behavior was recorded for 12 min after 2-µL of 30% 2-

nonanone (cat. no. 132-04173; Wako, Japan) diluted in 99.5% ethanol (cat. no. 0057-00456;

Wako, Japan) were placed at two spots on the surface of the NGM plate. This assay was

performed under the following three conditions: (1) Naive—the worms cultivated on 6-cm

NGM plates with the RRID:WB-STRAIN:OP-50 bacteria as food were briefly washed with

NGM buffer and subjected to the assay; (2) Pre-exposed—the worms were subjected to the

assay after being pre-exposed to 0.6 µL of 15% 2-nonanone spotted on the lid of a 6-cm NGM

plate for 1 h without food; and (3) Mock—the worms were subjected to the assay after being

pre-exposed to ethanol similarly to the pre-exposed condition. We added the mock-treated

control group to ensure that the starvation itself did not affect the odor avoidance behavior of

worms and to extract behavioral features modulated by odor pre-exposure compared with the

naive and mock-treated control groups. Images of worms on the 9-cm NGM plate during the odor avoidance assay were acquired by a high-resolution USB camera (DMK 72AUC02; The Imaging Source, USA) with a lens (LM16JC5MW; Kowa, Japan) at 1 Hz for 12 min. The coordinates of individual animals' centroids were acquired from the recorded images using the Move-tr/2D software (Library Co., Ltd., Tokyo, Japan) and used for the STEFTR analysis.

Similar to the other sensory behaviors of the worms, trajectories in the 2-nonanone avoidance behavior can be divided into two states: (1) "run"—a relatively long period of straight movement, and (2) "pirouette"—a period of short movements interrupted by frequent reversals and turns (Kimura et al., 2010; Pierce-Shimomura et al., 1999). The angular change per second was calculated from the centroid coordinates, and movements of 1 s with angular changes larger than 90° were classified as a turn. The histogram of turn intervals could be fitted to two exponentials, suggesting that the turn intervals are regulated by two probabilistic mechanisms (Pierce-Shimomura et al., 1999; Yamazoe-Umemoto et al., 2015). The time point at which the two exponentials intersected was defined as t_{crit}, and turn intervals longer or shorter than the t_{crit} were classified as runs or included in pirouettes, respectively. The t_{crit} was calculated for the control (i.e., naive and mock-treated) condition for wild-type and mutant strains. Excel (Microsoft) was used for the above calculations. The odor concentrations that the worms experienced at specific spatiotemporal points were calculated according to the dynamic odor gradient model based on the measured odor concentration (Tanimoto et al., 2017; Yamazoe-Umemoto et al., 2018).

Statistical analyses were performed with Prism ver. 5.0 for Mac OSX (GraphPad

Software, CA, USA) and R (The R Project). The sample size was determined based on the

previous report (Yamazoe-Umemoto et al., 2015). A part of the original data used in this study

had already been analyzed and published previously (Yamazoe-Umemoto et al., 2015), and re-

analyzed with the STEFTR method.

Penguins *(This experiment was performed by Kentaro Ito, Nobuo Kokubun, and Akinori*

Takahashi)

Fieldwork was performed on chick-rearing Adélie penguins at Hukuro Cove colony

(69°13′ S, 39°38′ E) in Lützow-Holm Bay, East Antarctica. GPS-depth loggers (GPL380-DT

or GPL400-D3GT, weighing 55-85 g; Little Leonardo, Japan) were deployed among 11

penguins during the period between 27 December 2016 and 10 January 2017 and recovered

from all the birds after 1-2 days. While the loggers were set to record GPS positions and depth

every second, they could not record GPS positions when the penguins were diving. Therefore,

we linearly interpolated the data, when necessary, to obtain GPS positions every 1 minute

before further analysis. See Kokubun et al. for methodological details (Kokubun et al., 2015).

This fieldwork was carried out in accordance with the recommendations of the Law relating to

Protection of the Environment in Antarctica. The protocol was approved by the Ministry of the

Environment, Government of Japan. The sample size was not predetermined.

Flying seabirds *(This experiment was performed by Katsufumi Sato and Ken Yoda)*

Fieldwork was performed on *Calonectris leucomelas* at Funakoshi-Ohshima Island (39°24'N, 141°59'E) between August and September in 2011, 2012, 2013, and 2015. GPS logger (GiPSy-2, 37 × 16 × 4 mm or GiPSy-4, 37 × 19 × 6 mm; TechnoSmArt, Roma, Italy) was attached to the back feathers of chick-rearing Streaked Shearwaters with Tesa$^{®}$ tape (Beiersdorf AG; GmbH, Hamburg, Germany) and cyanoacrylate glue (Loctite$^{®}$401; Henkel Ltd., Hatfield, UK). The loggers were housed in waterproof heat-shrink tubing and set to record one fix per minute. The total weight of the unit was 25 g, which was less than 5% of the mean mass of the birds in accordance with the suggested load limit for flying seabirds. After approximately two weeks of deployment, we recaptured and retrieved the loggers. See Yoda et al. for methodological details (Yoda et al., 2014). The study was carried out in accordance with the recommendations of the guidelines of the Animal Experimental Committee of Nagoya University. The protocol was approved by the Animal Experimental Committee of Nagoya University. The sample size was not predetermined. A part of the original data used in this study had already been analyzed and published previously (Yoda et al., 2014), and re-analyzed with the STEFTR method.

Rats *(This experiment was performed by Takuma Kitanishi)*

Locomotion data of an adult male Long Evans rat were obtained from the Collaborative Research in Computational Neuroscience (CRCNS; RRID:SCR_005608) data sharing website (https://crcns.org, hc-3 dataset, ec013 rat) (Mizuseki et al., 2014). The rat

foraged for randomly dispersed water or foods on an elevated open field (180 cm × 180 cm) for

17 - 53 min. The rat's position was tracked by monitoring two light-emitting diodes mounted

above the head with an overhead video camera at 30 Hz. The 30-Hz tracking data were

resampled to 39.0625 Hz for offline processing. This study was carried out in accordance with

the recommendations of the Regulations on Animal Experiments at Osaka City University. The

protocol was approved by the Animal Care and Ethics Committee of Osaka City University.

The sample size was not predetermined. The original data used in this study had already been

analyzed and published previously (Diba and Buzsáki, 2008; Mizuseki et al., 2009; 2014), and

re-analyzed with the STEFTR method.

Flies *(This experiment was performed by Daisuke Takaichi, Yuki Ishikawa, and Azusa*

Kamikouchi)

Fruit flies *D. melanogaster* were raised on standard yeast-based media at 25ºC and

40 - 60% relative humidity under a 12-hour light/dark cycle. *Canton-S* flies aged between 6-8

days after eclosion were used as a wild-type. After eclosion, the males were housed singly,

while females were housed in groups until the experiment.

The locomotion measurement was performed as described previously with minor

modifications (Kohatsu and Yamamoto, 2015; Kohatsu et al., 2011). Briefly, a male fly was

tethered with a metal wire on its dorsal thorax and positioned over an air-supported Styrofoam

ball (diameter, c. a. 6 mm). The locomotion trajectory of the fly was recorded by monitoring the

rotations of the Styrofoam ball using an optical computer mouse sensor (BSMRU21BK; BUFFALO INC., Nagoya, Japan). The sensor detected the movements of the ball in the horizontal (Δx) and vertical (Δy) directions, which correspond to lateral and forward movements of the male fly, respectively. The Δx and Δy values, together with timestamps, were sent to a computer at 60 Hz via an Arduino Due microcontroller (Switch Science, Japan) with a custom sketch program. The 60-Hz data were down-sampled to 4-Hz data for the information gain analysis. The measurements were obtained at 25±1°C and 50±10% relative humidity and within 4 hours after light onset.

Female pheromones were applied to the male fly by placing the female's abdomen in contact with the male's foreleg at the onset of the measurement. A manipulator (M-3333, Narishige, Tokyo, Japan) actuated a pipette with a volume of 200 μL (FUKAEKASEI Co., Ltd., China), in which a live female with her abdomen exposed toward a male fly was captured. We manually controlled the position of the manipulator to contact the female's abdomen to the male's foreleg. This contact procedure was omitted in the control experiments.

Visual stimulus was applied directly after pheromone application by starting horizontal movements of the female fly in front of the male fly as described (Kohatsu et al., 2011). The visual stimulus consisted of ten left-right horizontal movements of the female that lasted for 40 s. Each movement started with the female fly in the front of the male fly (i.e., center) and continued as the female fly moved left until it reached the left end of the rail (i.e., 5

mm away from the center), then moved right until it reached the right end of the rail (i.e., 5 mm away from the center), and ended when it came back to the center with a constant velocity of 5 mm/s. This movement was driven by a stepper motor (42BYG Stepper Motor, Makeblock Co., Ltd., Shenzhen, China) controlled by a custom sketch program (processing software version 3.3.7). We defined one round (4 s in total) as the movement related to the female starting to move away from the center, reaching the left end of the rail, passing the center, moving away to reach the right end of the rail, and coming back to the center again. Each of the "moving away" and "coming back" periods lasted for 1 s.

The Δx and Δy values with timestamps obtained in the final eight rounds were used for the analysis. To detect the characteristic parameters for the chasing behavior, we used Δx and Δy values during the period when the female was moving away from the male (2 s/round). We set the angle of the chasing behavior as 0 degree when the male moved forward. Angles between 0 and 90 degrees indicate that the male fly is moving towards the female that was moving away from the male.

As the parameters (velocity, bearing, and their time-differential values) were not normally distributed (Shapiro-Wilk test; see Supplementary Table 13), their values were compared between conditions (with/without pheromone) using the Mann-Whitney U test followed by Bonferroni correction for multiple comparisons. We used the Steel-Dwass test to compare values of the parameters between rounds. Statistical analyses were conducted using R

software version 3.4.4. No statistical methods were used to pre-determine sample sizes, but our sample sizes are similar to those in previous studies (Kohatsu and Yamamoto, 2015; Kohatsu et al., 2011).

Bats *(This experiment was performed by Yasufumi Yamada, and Shizuko Hiryu)*

Three adult Japanese horseshoe bats (*Rhinolophus ferrumequinum nippon*, body length: 6–8 cm, body mass: 20–30 g) were captured from natural caves in the Hyogo and Osaka prefectures in Japan as previously described (Yamada et al., 2016). The bats were housed in a temperature- and humidity-controlled colony room [4 m (L) × 3 m (W) × 2 m (H)] with a 12-h light/dark cycle at Doshisha University in Kyoto, Japan, and were allowed to fly freely and given access to mealworms and water. Captures were conducted under license and in compliance with current Japanese law. This study was carried out in accordance with the recommendations of Principles of Animal Care (publication no. 86-23 [revised 1985)] of the National Institutes of Health) and all Japanese laws. The protocol was approved by the Animal Experiment Committee of Doshisha University.

Methods for acoustic navigation measurement in bats have been described elsewhere (Yamada 2017). Briefly, the experiments were conducted in a flight chamber constructed using steel plates [9 (length) × 4.5 (width) × 2.5 m (height)] under lighting with red filters (>650 nm) to avoid visual effects on the bats. An obstacle environment was constructed using plastic chains (diameter: 4 cm) suspended from the ceiling of the chamber. The chains were arranged at

15-cm intervals along the *x*-axis and at 22-cm intervals along the *y*-axis so that the bat was

forced to fly in an S-shaped pattern without passing between chains. Three naive bats were

observed for 12 continuous repeated flights so that their echolocation behavior in unfamiliar and

familiar spaces could be compared. In this study, the first three flights were defined as

unfamiliar flights, while the last three flights were defined as familiar flights.

The flight behavior of the bats was recorded at 125 frames/s using two digital high-

speed video cameras (MotionPro X3; IDT Japan, Inc., Japan) placed in the left and right corners

of the flight chamber. Based on a direct linear transformation technique, the successive 3D

positions of the flying bats, as well as the locations of other objects, were reconstructed using

motion analysis software (DIPPMotionPro ver. 2.2.1.0; Ditect Corp., Japan). The statistical

calculations were performed with SPSS version 23 (IBM Corp.).

Calcium imaging of worm's neurons *(This experiment was performed by Yosuke Ikejiri)*

Calcium imaging of the worms' ASH neurons was performed according to the previous method

with some modifications (Tanimoto et al., 2017). Briefly, transgenic strains expressing

GCaMP3 (Tian et al., 2009) and mCherry (Shaner et al., 2004) in ASH sensory neurons under

the *sra-6* promoter (KDK70034 and KDK70072; 20 ng/µl of *sra-6p::GCaMP3*, 20 ng/µl of *sra-6p::mCherry*, 10 ng/µl of *lin-44p::GFP*, 50 ng/µl of PvuII-cut N2 genomic DNA as a carrier in

N2 background) were placed on an NGM agar plate on a robotic microscope system, OSB2

(Tanimoto et al., 2017). Although these transgenic worms were immobilized with the

acetylcholine receptor agonist levamisole (Lewis et al., 1980) for high-throughput data

acquisition through simultaneous imaging of multiple worms, the previous study revealed that

the ASH activity is essentially unaffected by levamisole-treatment (Tanimoto et al., 2017). A

constant gas flow of 8 mm/min was delivered, in which the mixture rate of 2-nonanone gas with

air was changed to create a temporal gradient of odor concentration. The temporal change in

odor concentration was measured by a custom-made semiconductor sensor before and after the

series of calcium imaging experiments on each day. The fluorescence signals of GCaMP3 and

mCherry in ASH neurons were divided into two channels using W-View (Hamamatsu, Japan),

an image splitting optic, and captured by an electron multiplying charge-coupled detector (EM-

CCD) camera (ImagEM; Hamamatsu, Japan) at 1 Hz. The intensities of fluorescence signals

from cell bodies were extracted and quantified by ImageJ (NIH) after background subtraction.

The average ratio over 30 s prior to the odor increase was used as a baseline (F_0), and the

difference from F_0 (ΔF) was used to calculate the fluorescence intensities of GCaMP3 and

mCherry ($F = \Delta F/F_0$). The ratio between florescence intensities of GCaMP and mCherry

(GCaMP/mCherry) was used in the figure.

REFERENCES

Alivisatos, A. P., Chun, M., Church, G. M., Greenspan, R. J., Roukes, M. L., and Yuste, R. (2012). The Brain Activity Map Project and the Challenge of Functional Connectomics. *Neuron* 74, 970–974. doi:10.1016/j.neuron.2012.06.006.

Anderson, D. J., and Perona, P. (2014). Toward a Science of Computational Ethology. *Neuron* 84, 18–31. doi:10.1016/j.neuron.2014.09.005.

Baek, J.-H., Cosman, P., Feng, Z., Silver, J., and Schafer, W. R. (2002). Using machine vision to analyze and classify Caenorhabditis elegans behavioral phenotypes quantitatively. *J Neurosci Methods* 118, 9–21.

Berg, H C, and D.A. Brown. (1972). Chemotaxis in Escherichia Coli Analysed by Three-Dimensional Tracking. *Nature* 239 500-504.

Bargmann, C. I. (2006). Chemosensation in C. elegans. *WormBook*, 1–29. doi:10.1895/wormbook.1.123.1.

Bargmann, C. I., Hartwieg, E., and Horvitz, H. R. (1993). Odorant-selective genes and neurons mediate olfaction in C. elegans. *Cell* 74, 515–527.

Bennison, A., Bearhop, S., Bodey, T. W., Votier, S. C., Grecian, W. J., Wakefield, E. D., et al. (2017). Search and foraging behaviors from movement data: A comparison of methods. *Ecol Evol* 8, 13–24. doi:10.1002/ece3.3593.

Berman, G. J. (2018). Measuring behavior across scales. *BMC Biol* 16, 23. doi:10.1186/s12915-018-0494-7.

Bishop, C. M. (2006). *Pattern Recognition and Machine Learning*. Springer Verlag.

Block, S M, J E Segall, and H C Berg. (1982). Impulse Responses in Bacterial Chemotaxis. *Cell* 31, 215–26.

Branson, K., Robie, A. A., Bender, J., Perona, P., and Dickinson, M. H. (2009). High-throughput ethomics in large groups of Drosophila. *Nat Meth* 6, 451–457.

doi:10.1038/nmeth.1328.

Brenner, S. (1974). The genetics of Caenorhabditis elegans. *Genetics* 77, 71–94.

Brown, A. E. X., and de Bivort, B. (2018). Ethology as a physical science. *Nat Phys* 14, 653–657. doi:10.1038/s41567-018-0093-0.

Brown, A. E. X., Yemini, E. I., Grundy, L. J., Jucikas, T., and Schafer, W. R. (2013). A dictionary of behavioral motifs reveals clusters of genes affecting Caenorhabditis elegans locomotion. *Proc Natl Acad Sci USA* 110, 791–796. doi:10.1073/pnas.1211447110.

Buhusi, C. V., and Meck, W. H. (2005). What makes us tick? Functional and neural mechanisms of interval timing. *Nat Rev Neurosci* 6, 755–765. doi:10.1038/nrn1764.

Colbert, H. A., Smith, T. L., and Bargmann, C. I. (1997). OSM-9, a novel protein with structural similarity to channels, is required for olfaction, mechanosensation, and olfactory adaptation in Caenorhabditis elegans. *J Neurosci* 17, 8259–8269.

Dankert, H., Wang, L., Hoopfer, E. D., Anderson, D. J., and Perona, P. (2009). Automated monitoring and analysis of social behavior in Drosophila. *Nat Meth* 6, 297–303. doi:10.1038/nmeth.1310.

De Bono, M., and Maricq, A. V. (2005). Neuronal substrates of complex behaviors in C. elegans. *Annu Rev Neurosci* 28, 451–501. doi:10.1146/annurev.neuro.27.070203.144259.

Dell, A. I., Bender, J. A., Branson, K., Couzin, I. D., de Polavieja, G. G., Noldus, L. P. J. J., et al. (2014). Automated image-based tracking and its application in ecology. *Trends in Ecology & Evolution* 29, 417–428. doi:10.1016/j.tree.2014.05.004.

Dempster, A. P., Laird, N. M., Rubin, D. B., 1977 (1977). Maximum likelihood from incomplete data via the EM algorithm. *J Royal Stat Soc B* 39, 1–38. doi:10.2307/3315718.

Diba, K., and Buzsáki, G. (2008). Hippocampal network dynamics constrain the time lag between pyramidal cells across modified environments. *J Neurosci* 28, 13448–13456. doi:10.1523/JNEUROSCI.3824-08.2008.

Egnor, S. E. R., and Branson, K. (2016). Computational Analysis of Behavior. *Annu Rev*

Neurosci 39, 217–236. doi:10.1146/annurev-neuro-070815-013845.

Frank, E., Hall, M. A., and Witten, I. H. (2016). "The WEKA Workbench (Online Appendix)," in *Data Mining* (Morgan Kaufmann).

Garriga, J., Palmer, J. R. B., Oltra, A., and Bartumeus, F. (2016). Expectation-Maximization Binary Clustering for Behavioural Annotation. *PLoS ONE* 11, e0151984–26. doi:10.1371/journal.pone.0151984.

Gomez-Marin, A., Paton, J. J., Kampff, A. R., Costa, R. M., and Mainen, Z. F. (2014). Big behavioral data: psychology, ethology and the foundations of neuroscience. *Nat Neurosci* 17, 1455–1462. doi:10.1038/nn.3812.

Gorelik, R., and Gautreau, A. (2014). Quantitative and unbiased analysis of directional persistence in cell migration. *Nat Protoc* 9, 1931–1943. doi:10.1038/nprot.2014.131.

Gurarie, E., Bracis, C., Delgado, M., Meckley, T. D., Kojola, I., and Wagner, C. M. (2016). What is the animal doing? Tools for exploring behavioural structure in animal movements. *J Anim Ecol* 85, 69–84. doi:10.1111/1365-2656.12379.

Iino, Y., and Yoshida, K. (2009). Parallel use of two behavioral mechanisms for chemotaxis in Caenorhabditis elegans. *J Neurosci* 29, 5370–5380. doi:10.1523/JNEUROSCI.3633-08.2009.

Jonsen, I. D., Basson, M., Bestley, S., Bravington, M. V., Patterson, T. A., Pedersen, M. W., et al. (2013). State-space models for bio-loggers: A methodological road map. *Deep Sea Research Part II: Topical Studies in Oceanography* 88–89, 34–46. doi:10.1016/j.dsr2.2012.07.008.

Kabra, M., Robie, A. A., Rivera-Alba, M., Branson, S., and Branson, K. (2013). JAABA: Interactive machine learning for automatic annotation of animal behavior. *Nat Meth* 10, 64–67. doi:10.1038/nmeth.2281.

Kaplan, J. M. (1996). Sensory signaling in Caenorhabditis elegans. *Curr Opin Neurobiol* 6, 494–499.

Kass, J., Jacob, T. C., Kim, P., and Kaplan, J. M. (2001). The EGL-3 proprotein convertase regulates mechanosensory responses of Caenorhabditis elegans. *J Neurosci* 21, 9265–9272.

Kimura, K. D., Fujita, K., and Katsura, I. (2010). Enhancement of odor avoidance regulated by dopamine signaling in Caenorhabditis elegans. *J Neurosci* 30, 16365–16375. doi:10.1523/JNEUROSCI.6023-09.2010.

Kohatsu, S., and Yamamoto, D. (2015). Visually induced initiation of Drosophila innate courtship-like following pursuit is mediated by central excitatory state. *Nature Communications* 6, 6457. doi:10.1038/ncomms7457.

Kohatsu, S., Koganezawa, M., and Yamamoto, D. (2011). Female contact activates male-specific interneurons that trigger stereotypic courtship behavior in Drosophila. *Neuron* 69, 498–508. doi:10.1016/j.neuron.2010.12.017.

Kokubun, N., Lee, W. Y., Kim, J.-H., and Takahashi, A. (2015). Chinstrap penguin foraging area associated with a seamount in Bransfield Strait, Antarctica. *Polar Science* 9, 393–400. doi:10.1016/j.polar.2015.10.001.

Komatsu, H., Mori, I., Rhee, J. S., Akaike, N., and Ohshima, Y. (1996). Mutations in a cyclic nucleotide-gated channel lead to abnormal thermosensation and chemosensation in C. elegans. *Neuron* 17, 707–718.

Krakauer, J. W., Ghazanfar, A. A., Gomez-Marin, A., MacIver, M. A., and Poeppel, D. (2017). Neuroscience Needs Behavior: Correcting a Reductionist Bias. *Neuron* 93, 480–490. doi:10.1016/j.neuron.2016.12.041.

Land, M., Islas-Trejo, A., and Rubin, C. S. (1994). Origin, properties, and regulated expression of multiple mRNAs encoded by the protein kinase C1 gene of Caenorhabditis elegans. *J. Biol. Chem.* 269, 14820–14827.

Landhuis, E. (2017). Neuroscience: Big brain, big data. *Nature* 541, 559–561. doi:10.1038/541559a.

Lee, R. Y., Sawin, E. R., Chalfie, M., Horvitz, H. R., and Avery, L. (1999). EAT-4, a homolog of a mammalian sodium-dependent inorganic phosphate cotransporter, is necessary for

glutamatergic neurotransmission in caenorhabditis elegans. *J Neurosci* 19, 159–167.

Lewis, J. A., Wu, C. H., Berg, H., and Levine, J. H. (1980). The genetics of levamisole resistance in the nematode Caenorhabditis elegans. *Genetics* 95, 905–928.

Lockery, S. R. (2011). The computational worm: spatial orientation and its neuronal basis in C. elegans. *Curr Opin Neurobiol* 21, 782–790. doi:10.1016/j.conb.2011.06.009.

Mathis, A., Mamidanna, P., Cury, K. M., Abe, T., Murthy, V. N., Mathis, M. W., et al. (2018). DeepLabCut: markerless pose estimation of user-defined body parts with deep learning. *Nat Neurosci*, 1–12. doi:10.1038/s41593-018-0209-y.

Matsumoto, S., Yamamoto, T., Yamamoto, M., Zavalaga, C. B., and Yoda, K. (2017). Sex-related differences in the foraging movement of streaked shearwaters calonectris leucomelas breeding on Awashima Island in the sea of Japan. *Ornithological Science* 16, 23–32. doi:10.2326/osj.16.23.

Mizuseki, K., Diba, K., Pastalkova, E., Teeters, J., Sirota, A., and Buzsáki, G. (2014). Neurosharing: large-scale data sets (spike, LFP) recorded from the hippocampal-entorhinal system in behaving rats. *F1000Res* 3, 98. doi:10.12688/f1000research.3895.1.

Mizuseki, K., Sirota, A., Pastalkova, E., and Buzsáki, G. (2009). Theta Oscillations Provide Temporal Windows for Local Circuit Computation in the Entorhinal-Hippocampal Loop. *Neuron* 64, 267–280. doi:10.1016/j.neuron.2009.08.037.

Moss, C. F., and Surlykke, A. (2010). Probing the natural scene by echolocation in bats. *Front Behav Neurosci* 4. doi:10.3389/fnbeh.2010.00033.

Nathan, R., Spiegel, O., Fortmann-Roe, S., Harel, R., Wikelski, M., and Getz, W. M. (2012). Using tri-axial acceleration data to identify behavioral modes of free-ranging animals: general concepts and tools illustrated for griffon vultures. *J Exp Biol* 215, 986–996. doi:10.1242/jeb.058602.

Nguyen, Jeffrey P, Frederick B Shipley, Ashley N Linder, George S Plummer, Mochi Liu, Sagar U Setru, Joshua W Shaevitz, and Andrew M Leifer. (2016). Whole-Brain Calcium Imaging with Cellular Resolution in Freely Behaving Caenorhabditis Elegans. *Proc Natl*

Acad Sci USA 113, 1074–1081. doi:10.1073/pnas.1507110112.

Patterson, T. A., Thomas, L., Wilcox, C., Ovaskainen, O., and Matthiopoulos, J. (2008). State-space models of individual animal movement. *Trends in Ecology & Evolution* 23, 87–94. doi:10.1016/j.tree.2007.10.009.

Pierce-Shimomura, J. T., Morse, T. M., and Lockery, S. R. (1999). The fundamental role of pirouettes in Caenorhabditis elegans chemotaxis. *J Neurosci* 19, 9557–9569.

Quinlan, J. R. (1986). Induction of Decision Trees. *Mach Learn* 1, 81–106. doi:10.1023/A:1022643204877.

Robie, A. A., Hirokawa, J., Edwards, A. W., Umayam, L. A., Lee, A., Phillips, M. L., et al. (2017). Mapping the Neural Substrates of Behavior. *Cell* 170, 393–406.e28. doi:10.1016/j.cell.2017.06.032.

Sasakura, H., and Mori, I. (2013). Behavioral plasticity, learning, and memory in C. elegans. *Curr Opin Neurobiol* 23, 92–99. doi:10.1016/j.conb.2012.09.005.

Shaner, N. C., Campbell, R. E., Steinbach, P. A., Giepmans, B. N. G., Palmer, A. E., and Tsien, R. Y. (2004). Improved monomeric red, orange and yellow fluorescent proteins derived from Discosoma sp. red fluorescent protein. *Nat Biotech* 22, 1567–1572. doi:10.1038/nbt1037.

Stephens, G. J., Johnson-Kerner, B., Bialek, W., and Ryu, W. S. (2008). Dimensionality and Dynamics in the Behavior of C. elegans. *PLoS Comput Biol* 4, e1000028. doi:10.1371/journal.pcbi.1000028.

Suo, S., Ishiura, S., and Van Tol, H. H. M. (2004). Dopamine receptors in C. elegans. *Eur. J. Pharmacol.* 500, 159–166. doi:10.1016/j.ejphar.2004.07.021.

Tanimoto, Y., Yamazoe-Umemoto, A., Fujita, K., Kawazoe, Y., Miyanishi, Y., Yamazaki, S. J., et al. (2017). Calcium dynamics regulating the timing of decision-making in C. elegans. *eLife* 6, e21629. doi:10.7554/eLife.21629.

Tian, L., Hires, S. A., Mao, T., Huber, D., Chiappe, M. E., Chalasani, S. H., et al. (2009). Imaging neural activity in worms, flies and mice with improved GCaMP calcium

indicators. *Nat Meth* 6, 875–881. doi:10.1038/nmeth.1398.

Tobin, D., Madsen, D., Kahn-Kirby, A., Peckol, E., Moulder, G., Barstead, R., et al. (2002). Combinatorial expression of TRPV channel proteins defines their sensory functions and subcellular localization in C. elegans neurons. *Neuron* 35, 307–318.

Venkatachalam, V., Ji, N., Wang, X., Clark, C., Mitchell, J. K., Klein, M., et al. (2016). Pan-neuronal imaging in roaming Caenorhabditis elegans. *Proc Natl Acad Sci USA* 113, 1082–1088. http://doi.org/10.1073/pnas.1507109113

Viswanathan, G M, E P Raposo, and M G E da Luz. (2008). Lévy Flights and Superdiffusion in the Context of Biological Encounters and Random Searches. *Physics of Life Reviews* 5, 133–150. doi:10.1016/j.plrev.2008.03.002.

Viswanathan, G M, V Afanasyev, S V Buldyrev, E J Murphy, P A Prince, and H E Stanley. (1996). Lévy Flight Search Patterns of Wandering Albatrosses. *Nature* 381, 413-415. doi:10.1038/381413a0.

Vogelstein, J. T., Park, Y., Ohyama, T., Kerr, R. A., Truman, J. W., Priebe, C. E., et al. (2014). Discovery of Brainwide Neural-Behavioral Maps via Multiscale Unsupervised Structure Learning. *Science* 344, 386–392. doi:10.1126/science.1250298.

Watanabe, S., Sato, K., and Ponganis, P. J. (2012). Activity time budget during foraging trips of emperor penguins. *PLoS ONE* 7, e50357. doi:10.1371/journal.pone.0050357.

White, J. G., Southgate, E., Thomson, J. N., and Brenner, S. (1986). The Structure of the Nervous System of the Nematode Caenorhabditis elegans. *Philosophical Transactions of the Royal Society B: Biological Sciences* 314, 1–340. doi:10.1098/rstb.1986.0056.

Wiltschko, A. B., Johnson, M. J., Iurilli, G., Peterson, R. E., Katon, J. M., Pashkovski, S. L., et al. (2015). Mapping Sub-Second Structure in Mouse Behavior. *Neuron* 88, 1121–1135. doi:10.1016/j.neuron.2015.11.031.

Yamada, Y. (2017). A study on cheap robust sensing for obstacle avoidance guidance based on bio-sonar strategy of bats. Ph.D. Thesis. doi:10.14988/di.2017.0000016957.

Yamada, Y., Hiryu, S., and Watanabe, Y. (2016). Species-specific control of acoustic gaze by

echolocating bats, Rhinolophus ferrumequinum nippon and Pipistrellus abramus, during flight. *J Comp Physiol A* 202, 791–801. doi:10.1007/s00359-016-1121-0.

Yamamoto, D., and Koganezawa, M. (2013). Genes and circuits of courtship behaviour in drosophila males. *Nat Rev Neurosci* 14, 681–692. doi:10.1038/nrn3567.

Yamazoe-Umemoto, A., Fujita, K., Iino, Y., Iwasaki, Y., and Kimura, K. D. (2015). Modulation of different behavioral components by neuropeptide and dopamine signalings in non-associative odor learning of Caenorhabditis elegans. *Neurosci Res* 99, 22–33. doi:10.1016/j.neures.2015.05.009.

Yamazoe-Umemoto, A., Iwasaki, Y., and Kimura, K. (2018). Measuring Spatiotemporal Dynamics of Odor Gradient for   Small Animals by Gas Chromatography. *BIO-PROTOCOL* 8. doi:10.21769/bioprotoc.2797.

Yoda, K. (2018). Advances in bio-logging techniques and their application to study navigation in wild seabirds. *Advanced Robotics* 58, 1–10. doi:10.1080/01691864.2018.1553686.

Yoda, K., Naito, Y., Sato, K., Takahashi, A., Nishikawa, J., Ropert-Coudert, Y., et al. (2001). A new technique for monitoring the behaviour of free-ranging Adélie penguins. *Journal of Experimental Biology* 204, 685–690.

Yoda, K., Shiomi, K., and Sato, K. (2014). Foraging spots of streaked shearwaters in relation to ocean surface currents as identified using their drift movements. *Progress in Oceanography* 122, 54–64. doi:10.1016/j.pocean.2013.12.002.

Zhang, S. X., Miner, L. E., Boutros, C. L., Rogulja, D., and Crickmore, M. A. (2018). Motivation, Perception, and Chance Converge to Make a Binary Decision. *Neuron* 99, 376–388.e6. doi:10.1016/j.neuron.2018.06.014.

Zheng, Y. (2015). Trajectory Data Mining. *ACM Trans. Intell. Syst. Technol.* 6, 1–41. doi:10.1145/2743025.
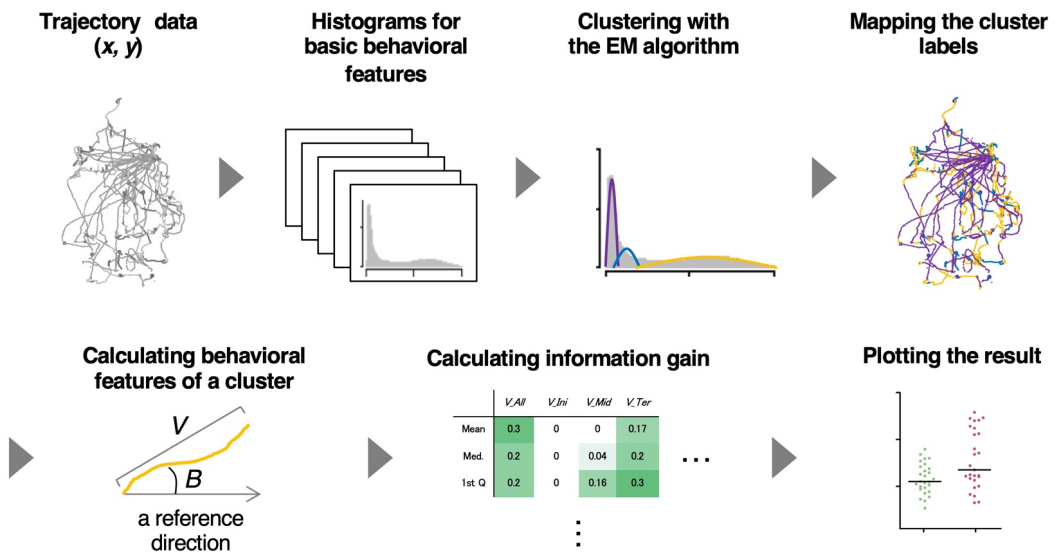
Figure 1. A workflow of the STEFTR method. Trajectory data of animals are used to calculate 8 basic behavioral features, and one of them is analyzed by the EM algorithm to estimate behavioral states (upper panels). From a behavioral state, behavioral features are comprehensively evaluated by using information gain (lower panels).
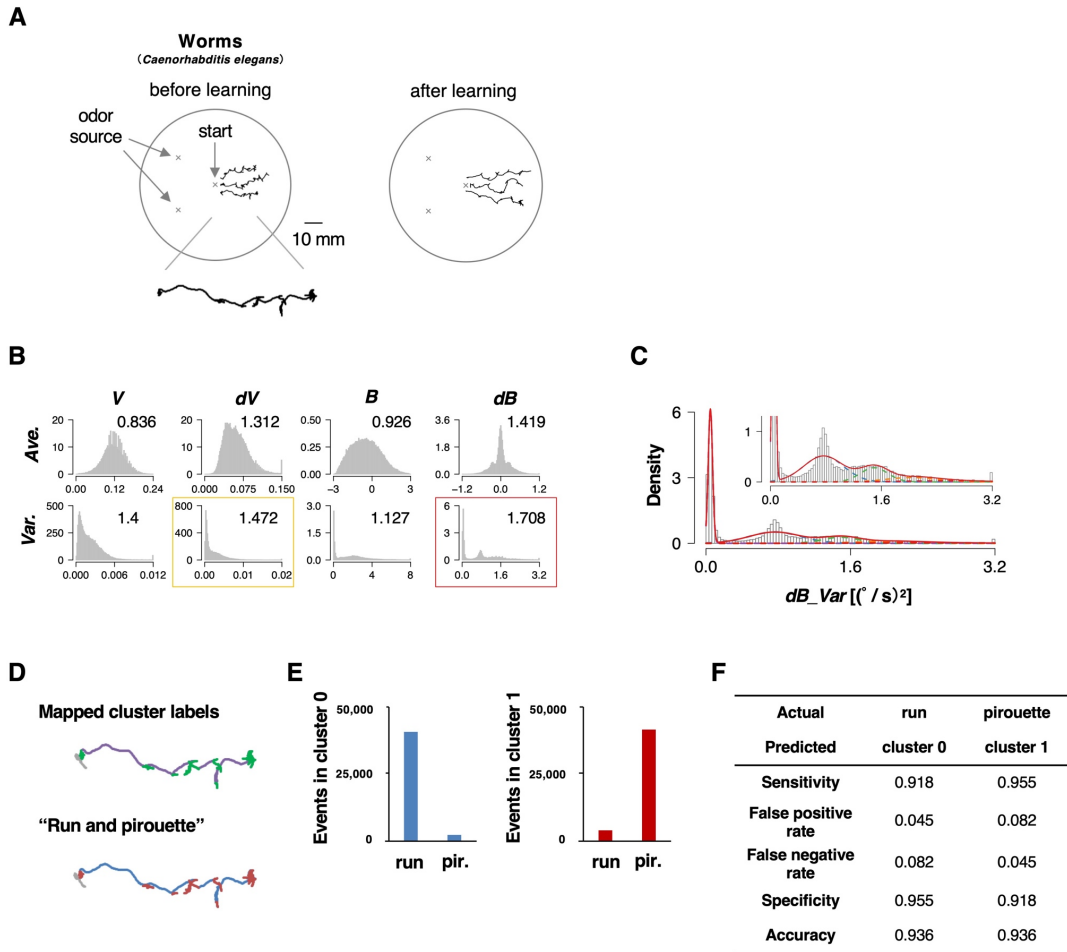
Figure 2. State estimation of worms. (A) Examples of the trajectories of 3 worms before (left) or after odor learning (right) in 12 min of 2-nonanone avoidance assay, overlaid on a schematic drawing of a 9 cm plate. One of the trajectories is magnified below. (B) The histograms of 8 basic behavioral features. Horizontal and vertical axes indicate the values and the density of each feature. The numbers in each panel indicate the separation indices. The red and yellow rectangles indicate the 1st and 2nd best separation indices, respectively. *dB_Var* was chosen (red square) for the EM analysis. (C) Clustering *dB_Var* by the EM algorithm. Each cluster

distribution (cluster 0, 1, 2, 3, and 4 are indicated by purple, blue, green, orange, and red dashed lines, respectively, similarly to the following figures) and the sum of clusters (red solid line) are shown. Inset is a magnified view. (D) Comparison of the cluster 0 and 1 (upper panel; purple and green, respectively) with run and pirouette (lower panel; blue and red, respectively) on a trajectory. The initial 2 minutes (gray in both panels) were excluded from the analyses because worms do not avoid the odor during the period (Kimura et al., 2010). (E) Event numbers of cluster 0 (left) and 1 (right) in run and pirouette. (F) Matching matrix of the state estimation shows the followings: sensitivity = TP / (TP + FN), false positive rate = FP / (FP + TN), false negative rate = FN / (FN + TP), specificity = TN / (TN + FP) , accuracy = (TP + TN) / (TP + TN + FP + FN), where TP = true positive, TN = true negative, FP = false positive, FN = false negative.

This data was recorded by Akiko Yamazoe-Umemoto and Kosuke Fujita.
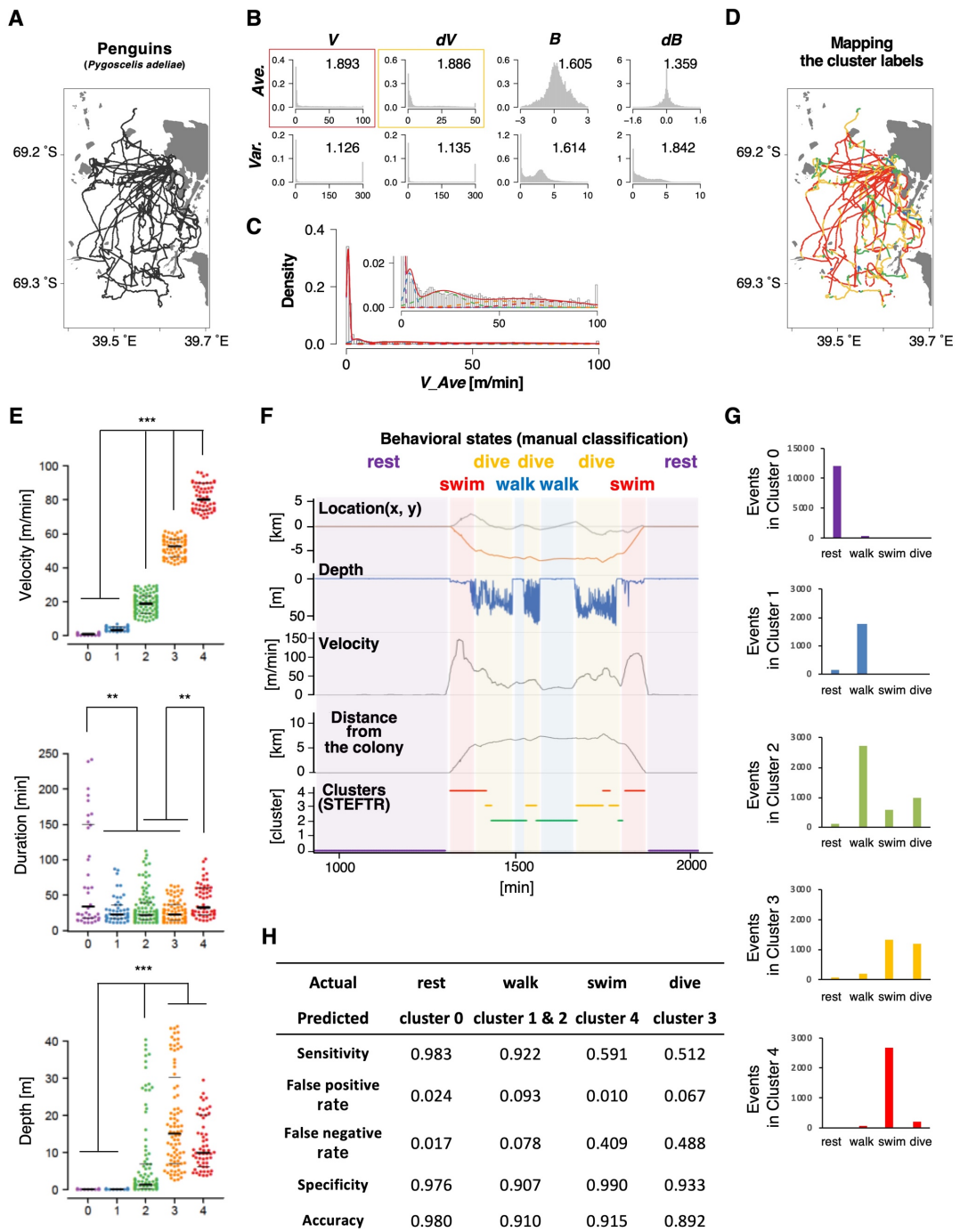
Figure 3. State estimation of penguins. (A) The trajectories of 11 penguins (black lines) on the Antarctic Continent (gray area; white area is the sea). Horizontal and vertical axes indicate longitude and latitude, respectively. (B) The histograms of 8 basic behavioral features (upper panels) and the classification by the EM algorithm. The numbers in each panel indicate the

separation indices. The red and yellow rectangles indicate the 1st and 2nd best separation indices, respectively. (C) Clustering V_Ave into 5 clusters (D) Mapping of the 5 clusters on the trajectory. (E) Differences in velocity, duration, and depth among the clusters. Each dot represents a cluster bout, and the bars represent the median and the first and third quartiles. Significant differences among clusters suggest that the clusters correspond to different behavioral states. Statistical values were calculated using Kruskal-Wallis test with *post hoc* Dunn's test. **$p < 0.01$, ***$p < 0.001$. (F) An example of comparison of the clusters from the STEFTR analysis with the behavioral states by manually classified labels, which is based on diving depth, movement speed recorded from GPS data, and distance from the colony. (G) Event numbers of each cluster. (H) Matching matrix of the state estimation. The statistical details are described in Supplementary Table 1.

This data was recorded by Kentaro Ito, Nobuo Kokubun, and Akinori Takahashi.
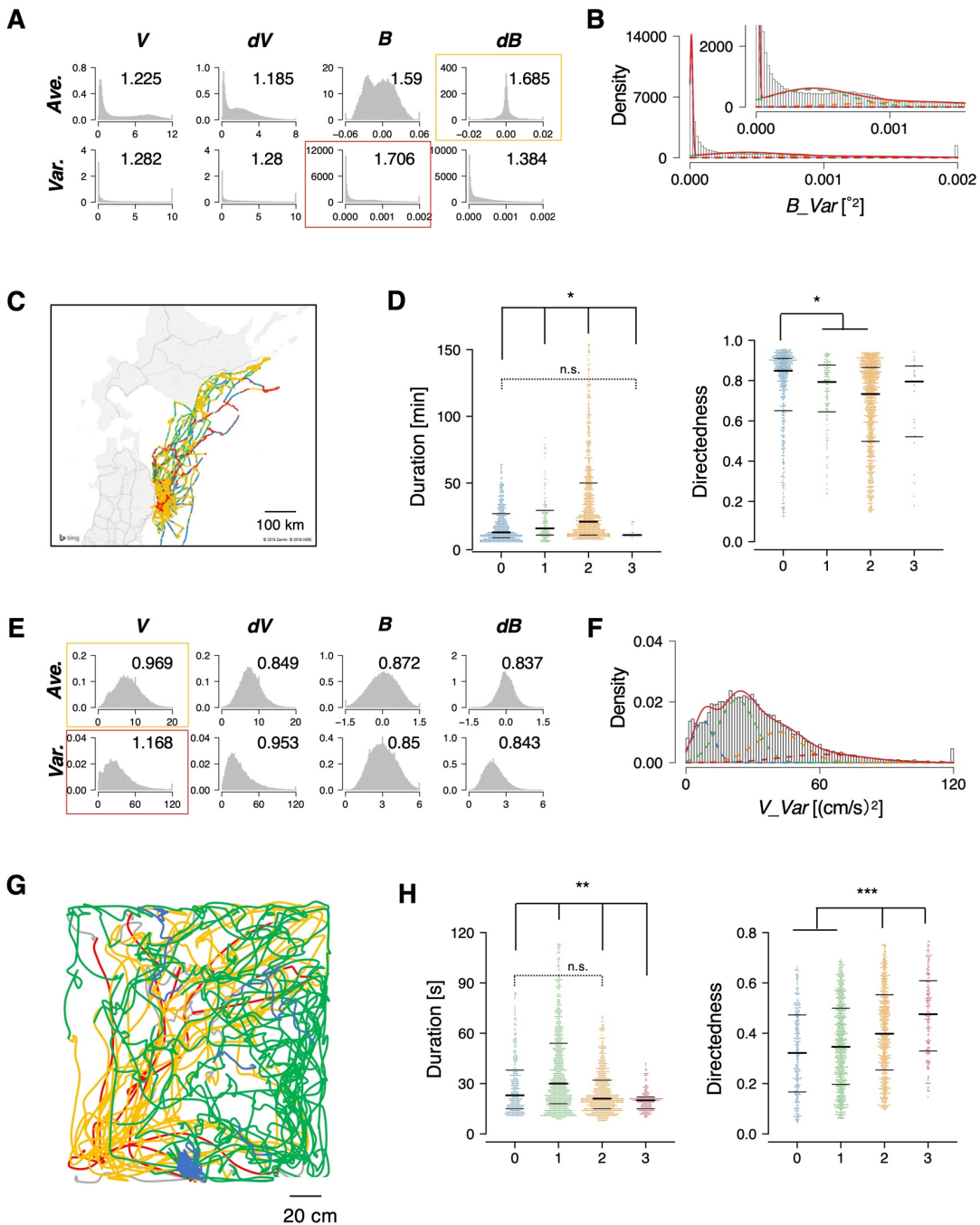
Figure 4. State estimation of flying seabirds in the Pacific Ocean. (A-D) and rats in the open

maze (E-H). (A) 8 basic features of flying seabirds. (B) Clustering *B_Var* into 4 clusters. (C)

Mapping of the clusters on the trajectory. The gray region is the northern part of Japan (Tohoku

and Hokkaido area), while the white region is the sea. (D) Significant differences were observed

in duration (left) and directedness (right). (E) Eight basic features of rats. (F) Clustering *V_Var* into 4 clusters. (G) An example of trajectories of one rat. (H) Significant differences were observed in duration (left) and directedness (right). Each dot represents a cluster bout, and the bars represent the median and the first and third quartiles. Statistical values were calculated using Kruskal-Wallis test with *post hoc* Dunn's test. $*p < 0.05$, $**p < 0.01$, $***p < 0.001$. The statistical details are described in Supplementary Table 1.

This data was recorded by Katsufumi Sato, Ken Yoda, and Takuma Kitanishi.

A

All

Ini *Mid* *Ter*

$Directedness = \dfrac{\text{- - - -}}{\sim}$

B

Low — | V_Ini | — High

(347, 349)
naive ≈ preexp

(234, 108)
naive > preexp

(113, 241)
naive < preexp

Parameter	naive Low	naive High	preexp Low	preexp High	entropy	Info gain
Original	347		349		1[a]	-
V_Ini	234	113	108	241	0.9017[b]	0.0983[c]

(*c* = *a* − *b*)
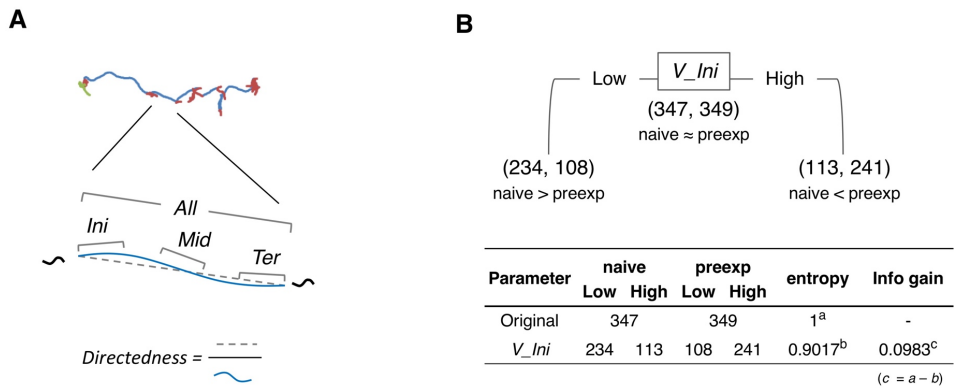
Figure 5. Feature extraction of worm behavior. (A) Schematic drawing of the behavioral features. (B) One example (*V_Ini*; average of time window 2) of calculation of information gain.
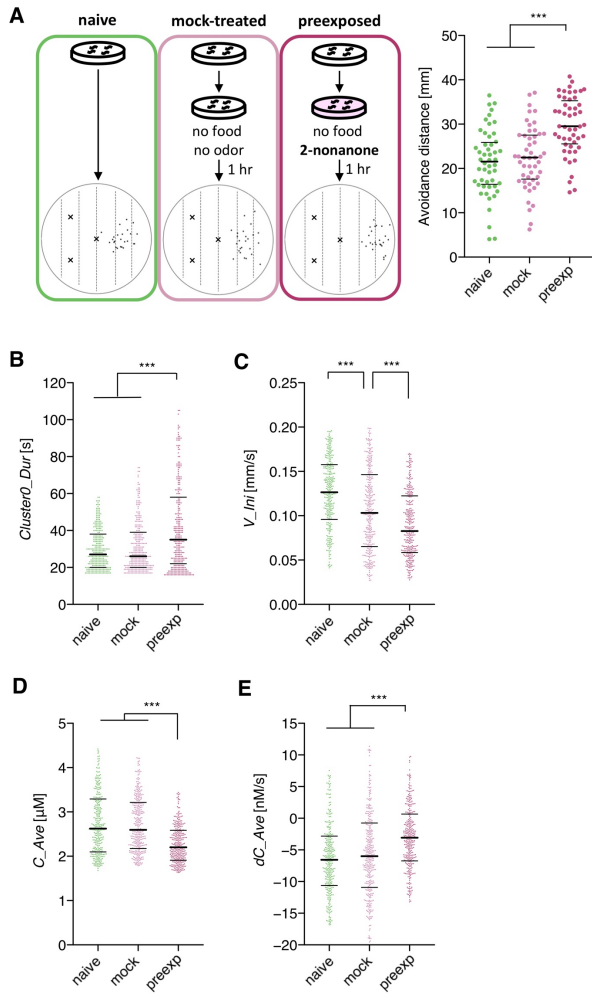
Figure 6. Extracted features modulated by the odor learning. (A) Enhanced odor avoidance behavior in worms caused by odor pre-exposure. Left: End-points of 25 worms in each condition plotted on a schematic representation of the assay plate. Right: Avoidance distance (distance between the center line of the plate and the end-point of the behavior) of each worm. Each dot represents a worm. Significant differences were observed between the pre-exposed worms and the naive and mock-treated worms (***p < 0.001, Kruskal-Wallis test with *post-hoc* Dunn's test). (B, C, D, and E) Distributions of extracted features. Duration (B), the initial value of velocity (C; average of time window 2), the average odor concentration (D), and the average odor concentration change (E) of each run (***p < 0.001, Kruskal-Wallis test with *post-hoc* Dunn's test). Each dot represents a cluster bout, and the bars represent the median and the first and third quartiles. The statistical details are described in Supplementary Table 1.

This data was recorded by Akiko Yamazoe-Umemoto and Kosuke Fujita.
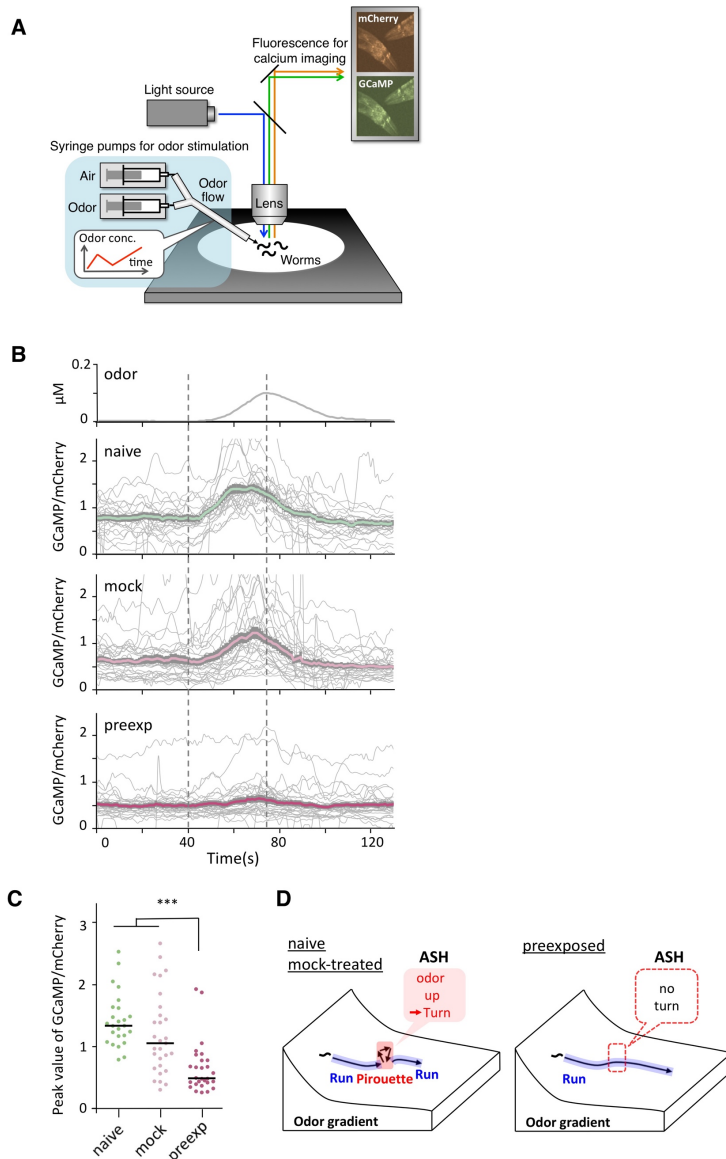
Figure 7. Sensory responses to slight increases in odor concentration were reduced by pre-exposure to the odor. (A) A schematic drawing of calcium imaging of neural activity of worms under odor stimuli. Several immobilized worms were simultaneously exposed to an odor flow whose concentration was changed by controlling syringe pumps. (B) Responses (GCaMP/mCherry) of ASH neurons in naive (n = 25), mock-treated (n = 29), and pre-exposed (n = 26) worms. Thick lines with gray shadows indicate mean ± standard error of the mean,

while thin lines indicate individual responses. (C) Distributions of peak values during the odor-increasing phase ($t = 40\text{-}80$ s) shown in panel B. The bars represent the median. (***$p < 0.001$, Kruskal-Wallis test with *post-hoc* Dunn's test). (D) A model relationship between odor concentration change and behavioral response during navigation along the odor gradient. When naive and mock-treated worms sensed a slight increase in the odor concentration, which is a sign of migrating in the wrong direction, they stopped a run and started a pirouette to search for a new direction. In contrast, the pre-exposed worms did not respond to a slight increase in odor concentration, leading to longer run durations (and shorter pirouette durations in total as a consequence), which likely contribute to the enhanced avoidance distance. The statistical details are described in Supplementary Table 1.

This experiment was performed by Yosuke Ikejiri.
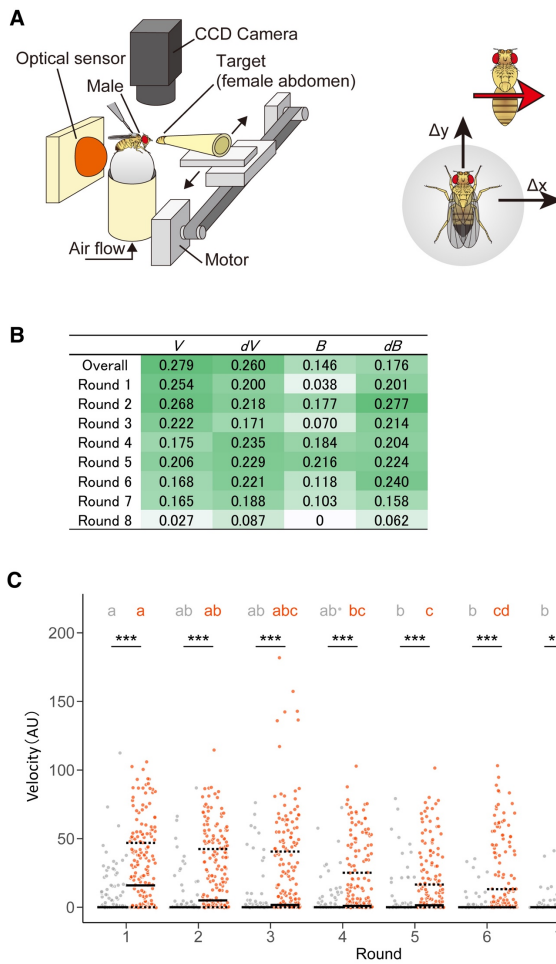
Figure 8. Pheromone-driven responses of male fruit flies decreased over time. (A) A schematic drawing of the experimental setup. A female fly was actuated leftward and rightward in front of the male fly. The locomotion of the male fly was monitored by an optical sensor, which recorded lateral (Δx) and forward (Δy) movements at 4 Hz. (B) Information gain. Darker and lighter colors mean larger and smaller values, respectively. (C) Distribution of velocity in the chasing behavior of male flies. Control (without female tapping, gray dots) and experimental (with female tapping, orange dots) groups are shown. Solid and dotted lines represent the median and the first and third quartiles, respectively. Asterisks indicate the statistical significance between the control and test groups (Mann-Whitney U test followed by Bonferroni test for multiple comparison correction, p < 0.05). Different characters in each group indicate statistical significance among rounds (Steel-Dwass test, $p < 0.05$). The statistical details are described in Supplementary Tables 12 and 13.

This data was recorded by Daisuke Takaichi, Yuki Ishikawa, and Azusa Kamikouchi.
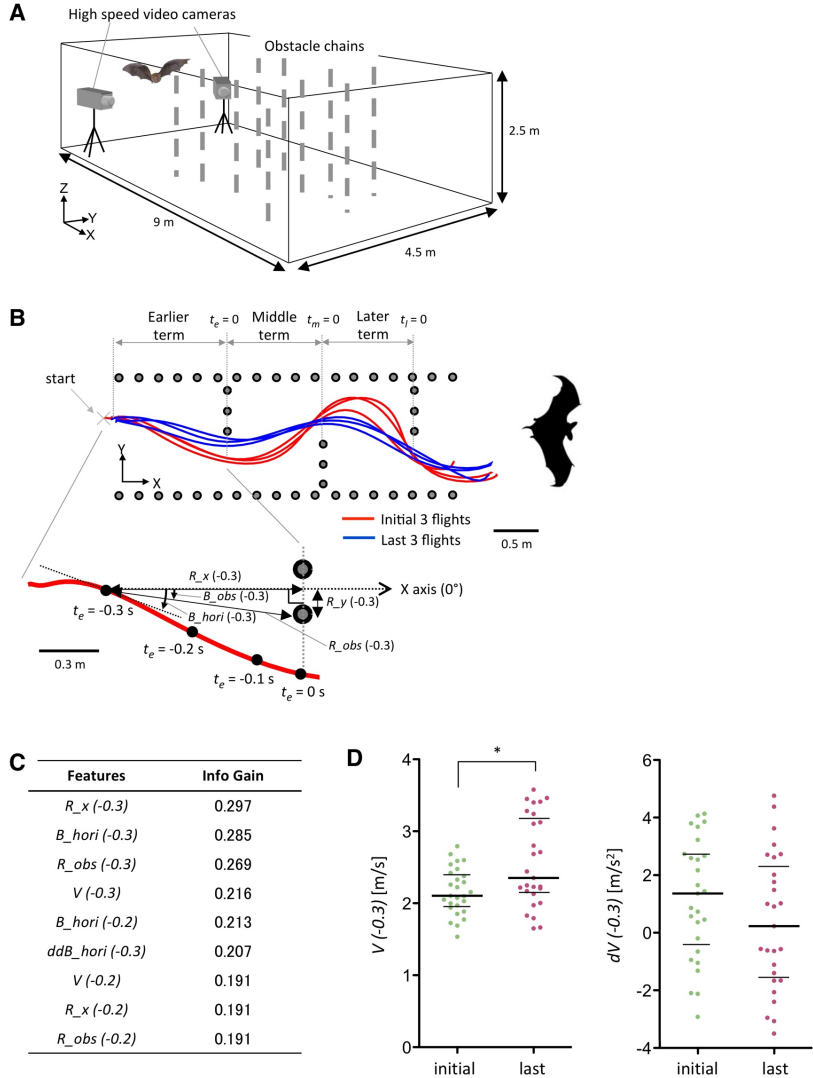
Figure 9. Learning-dependent changes in bat acoustic navigation. (A) The experimental setup for monitoring the 3D flight trajectory of a bat during obstacle avoidance flight in a chamber. (B) Representative flight trajectories of a bat in the horizontal plane during repeated flights in the obstacle course. The figure on the top combines the first three (red) and last three (blue) flight trajectories. Each behavioral feature was collected in three segments: earlier, middle, and later terms. The figure on the bottom shows an expanded view of the earlier term in the first flight. Definition of the horizontal bearing of the flight (*B_hori*), distance (*R_obs*), and bearing (*B_obs*) of the bat to the nearest edge point of the obstacle chain array, longitudinal directional distance to the frontal chain array (*R_x*), and lateral directional distance to the inside

pitch of the chains array (R_y) are indicated. Time windows for the analysis of each behavioral feature were 0.1, 0.2, or 0.3 s before or while ($t = 0$) passing through the chain array. (C) A list of extracted features of bat acoustic navigation modulated by flight experience. (D) Distributions of *V(-0.3)* and *dV(-0.3)* are plotted. The bars represent the median and the first and third quartiles. (*$p < 0.05$, Kruskal-Wallis test with *post-hoc* Dunn's test). The statistical details are described in Supplementary Table 1.

This data was recorded by Yasufumi Yamada and Shizuko Hiryu.

Table 1. Summary of recording and analysis conditions of animal behavior.

Animal	worms	penguins	flying seabirds	rats	flies	bats
Condition	naive, mock, preexposed	1	1	1	with or without pheromone	with or without learning
Animal # / condition	50 each	11	54	1	27, 30	3 each
Trajectory # / condition	50 each	11	54	45	27, 30	9 each
Recording time (min-max)	600 s	1626-2787 min	484-8293 min	1031-3194 s	16 s	1.67-2.53 s
Recording time (median)	600 s	2279 min	972 min	1822 min	16 s	1.95 s
Time unit	1 s	1 min	1 min	1 s	0.25 s	0.008 s
Time window for moving average	12 s	20 min	10 min	20 s	-	-
Feature used for EM	*dB_Var*	*V_Ave*	*B_Var*	*V_Var*	-	-
Length unit	mm	m	km	cm	a.u.	m
Approx. distance (min-max)	5-30 mm	1-10 km	100-2000 km	180 × 180 cm	1 - 500 mm	6 m

Table 2. Learning-dependent features extracted from cluster 0 in odor avoidance behavior of wild-type worms.

time	value	Clst0 Dur	Clst1 Dur	V				dV				B				dB				Dir				C				dC				WV
		All	All	All	Ini	Mid	Ter	All	Ini	Mid	Ter	All	Ini	Mid	Ter	All	Ini	Mid	Ter	All	Ini	Mid	Ter	All	Ini	Mid	Ter	All	Ini	Mid	Ter	All
-	Ave	0.098	0.057	-	-	-	-	-	-	-	-	-	-	-		0.072	-	-	-	-	-	-	-	0.163	-	-	-	0.088	-	-	-	
-	Med	-	-	0.040	-	-	-	-	-	-	-	-	-	-		0.102	-	-	-	-	-	-	-	0.160	-	-	-	0.088	-	-	-	
-	Q1st	-	-	-	-	-	-	-	-	-	-	-	-	-		0.065	-	-	-	-	-	-	-	0.164	-	-	-	0.107	-	-	-	
-	Q3rd	-	-	-	-	-	-	-	-	-	-	-	-	-		0.083	-	-	-	-	-	-	-	0.161	-	-	-	0.080	-	-	-	
-	Var	-	-	-	-	-	-	-	-	-	-	-	-	-		-	-	-	-	-	-	-	-		-	-	-	0.080	-	-	-	
-	1 %ile	-	-	-	-	-	-	-	-	-	-	-	-	-		-	-	-	-	-	-	-	-	0.163	-	-	-	0.090	-	-	-	
-	5 %ile	-	-	-	-	-	-	-	-	-	-	-	-	-		-	-	-	-	-	-	-	-	0.165	-	-	-	0.100	-	-	-	
-	95 %ile	-	-	-	-	-	-	-	-	-	-	-	-	-		-	-	-	-	-	-	-	-	0.153	-	-	-	0.108	-	-	-	
-	99 %ile	-	-	-	-	-	-	-	-	-	-	-	-	-		-	-	-	-	-	-	-	-	0.148	-	-	-	0.060	-	-	-	
1	Ave	-	-	-	0.114			-				-				-				-				-	0.147	0.162	0.162	-	0.116	0.093	0.104	-
2	Ave	-	-	-	0.120		0.049	-				-				-		0.048		-				-	0.148	0.166	0.163	-	0.111	0.105	0.122	-
3	Ave	-	-	-	0.109			-				-				-		0.049		-				-	0.151	0.163	0.162	-	0.110	0.099	0.128	-
3	Med	-	-	-	0.100		0.039	-				-				-				-				-	0.149	0.162	0.162	-	0.114	0.089	0.134	-
3	Var	-	-	-				-				-				-				-				-	0.111	0.087	0.041	-		0.060	0.050	-
4	Ave	-	-	-	0.099			-				-				-		0.050		-				-	0.147	0.166	0.165	-	0.082	0.098	0.122	-
4	Med	-	-	-	0.100			-				-				-				-				-	0.149	0.166	0.165	-	0.085	0.097	0.145	-
4	Var	-	-	-				-				-				-				-				-	0.102	0.083	0.040	-	0.057	0.082	0.082	-
5	Ave	-	-	-				-				-				-		0.048		-				-	0.146	0.163	0.166	-	0.090	0.112	0.148	-
5	Med	-	-	-	0.078			-				-				-				-				-	0.148	0.162	0.165	-	0.093	0.110	0.125	-
5	Var	-	-	-				-				-				-				-				-	0.097	0.092	0.054	-	0.061	0.112	0.078	-
6	Ave	-	-	-	0.072			-				-				-		0.056		-				-	0.148	0.164	0.146	-	0.083	0.112	0.169	-
6	Med	-	-	-	0.075			-				-				-				-				-	0.148	0.166	0.147	-	0.085	0.111	0.149	-
6	Var	-	-	-				-				-				-				-				-	0.089	0.095	0.060	-		0.116	0.081	-

Numbers are the sum of information gains obtained from the comparisons of naive vs. preexp. and mock. vs. preexp. Darker and lighter colors correspond to larger and smaller values, respectively. Blank cells, no value for information gain was obtained. "-", not calculated.

Table 3. Patterns of learning-dependent behavioral features of cluster 0 in odor avoidance behavior of mutant worms.

Strain	Clst0 Dur	Clst1 Dur	V				dV				B				dB				Dir				C				dC			
	All	All	All	Ini	Mid	Ter	All	Ini	Mid	Ter	All	Ini	Mid	Ter	All	Ini	Mid	Ter	All	Ini	Mid	Ter	All	Ini	Mid	Ter	All	Ini	Mid	Ter
wild-type	Up	D/U	Down	Down		Down									Down		Down						Down	Down	Down	Down	Up	Up	Up	Up
egl-3(n589)																							Up	Up	Up	Up				
egl-3(ok979)			Down	Down	Down	Down																	Up	Up	Up	Up				
egl-21																														
dop-3	Up		Down		Down	Down					Up		Up	Up				Up	Down		Down						Up		Up	Up
ocr-2			Up			Up																								
osm-9	Up		Up	Up	Up	Up																								
tax-4						Down									Down	U/D							D/U	D/U	D/U	D/U				
eat-4			Down	Down		Down																	Down							
pkc-1															Down		Down						Up				Down			

Darker and lighter colors mean larger and smaller information gain values, respectively. "Up" and "Down" indicates the value changes of pre-exposed worms compared with naive and mock-treated worms. "U/D" or "D/U" indicates the value of pre-exposed worms is higher than naive and lower than mock-treated worms, and *vice versa*. Blank cells, no value for information gain was obtained. The details of information gain are described in Supplementary Tables 2-11.

SUPPLEMENTARY FIGURES AND TABLES

A

Predicted	Actual	
cluster	run	pir.
0	**41,137**	1,950
1	3,291	**18,738**
2	339	**13,236**
3	62	**6,956**
4	1	**2,091**

B

Predicted	Actual	
cluster	run	pir.
0	**40,099**	11,298
1	3,150	**14,727**
2	1,409	**15,092**

C

Mapped cluster labels

"Run and pirouette"

D

E
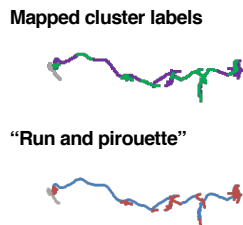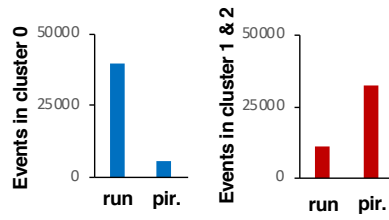
Predicted	Actual	
cluster	run	pir.
0	2,778	2,625
1	10,826	6,917
2	21,607	21,182
3	7,342	10,143
4	2,858	2,811

Supplementary Figure 1. State estimation of worms (Related to Figure 2). (A) Confusion matrix for the state estimation with *dB_Var*. (B-D) The results of state estimation with *dV_Var* in confusion matrix, where the histogram was separated to 3 clusters. (B) Confusion matrix. (C) Mapping on a trajectory. (D) Event numbers of run and pirouette in cluster 0 (left) and 1 & 2 (right). (E) Confusion matrix for the state estimation by *dB_Var* in finer (0.15%) window.

A

Predicted	Actual			
cluster	rest	walk	swim	dive
0	**12,177**	212	-	-
1	152	**1,763**	-	-
2	125	**2,743**	561	963
3	1	166	**1,304**	1,210
4	-	2	**2,691**	190

B

Predicted	Actual			
cluster	rest	walk	swim	dive
0	8,861	1,225	189	-
1	3,510	1,278	71	-
2	321	2,544	3,766	2,205
3	-	46	441	157
4	-	4	203	13

C

D
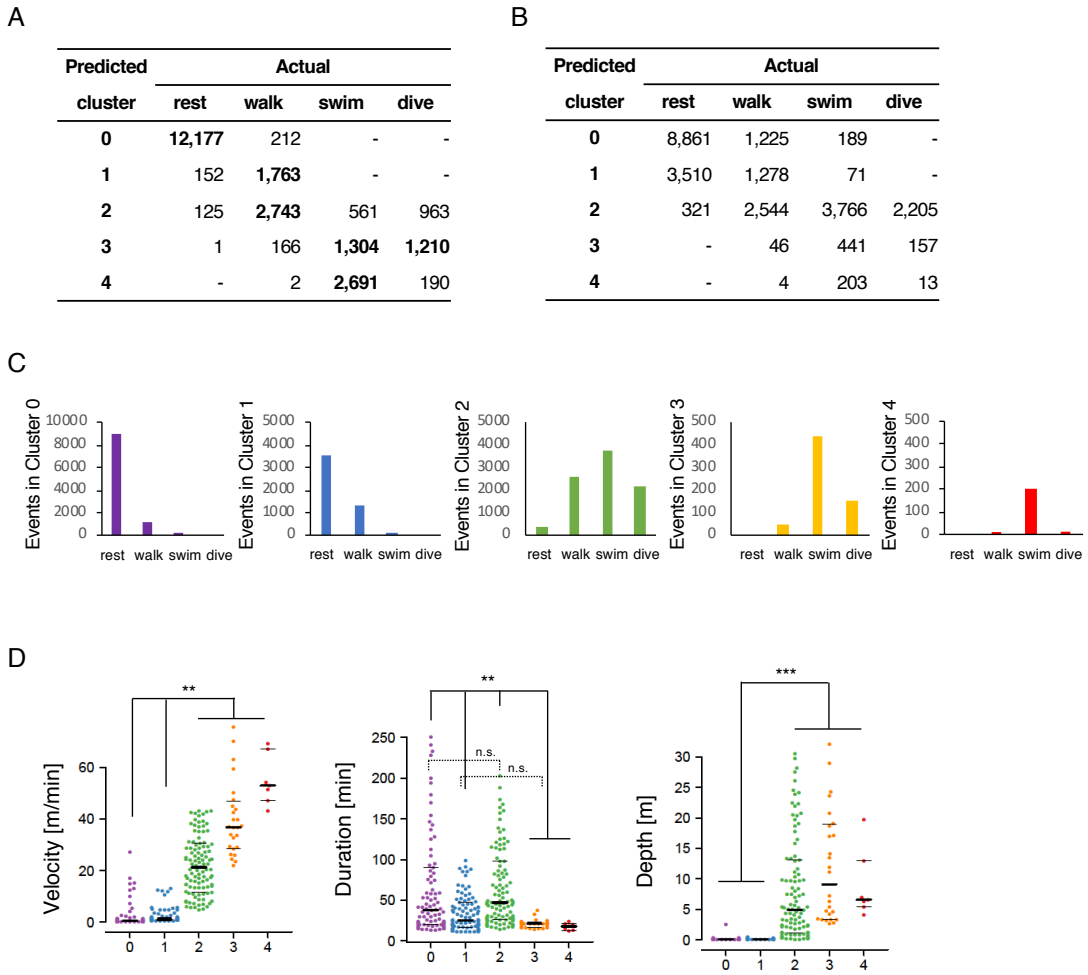
Supplementary Figure 2. State estimation of penguins (Related to Figure 3). (A) Confusion matrix for the state estimation with *dV_Ave*. (B-D) The results of state estimation with *dV_Ave* in confusion matrix (B) and event numbers of each cluster (C). (D) Differences in velocity, duration, and depth among the clusters with *dV_Ave*. Each dot represents a cluster bout, and the bars represent the median and the first and third quartiles. Statistical values were calculated using Kruskal-Wallis test with *post hoc* Dunn's test. **$p < 0.01$, ***$p < 0.001$.

Supplementary Table 1. Detailed results of statistical tests for Fig. 3-7, 9 and S2.

Figure	Parameter	Number of Groups	Group 1	Group 2	Group 3	Group 4	Group 5	Unit of number	Statistical tests used	p value of multiple test	Other result of multiple test	Post-hoc test	p value of post-hoc test	Other result of post-hoc test
3E	Velocity	5	cluster 0 (n=48)	cluster 1 (n=54)	cluster 2 (n=121)	cluster 3 (n=94)	cluster 4 (n=64)	clusters	Kruskal-Wallis test	<0.0001(***)	355.614	Dunn's test	0 vs 1: 0.1062(ns)	z = -2.3037
													0 vs 2: <0.0001(***)	z = -7.2863
													1 vs 2: <0.0001(***)	z = -4.8022
													0 vs 3: <0.0001(***)	z = -12.5996
													1 vs 3: <0.0001(***)	z = -10.4138
													2 vs 3: <0.0001(***)	z = -7.2173
													0 vs 4: <0.0001(***)	z = -15.3219
													1 vs 4: <0.0001(***)	z = -13.3596
													2 vs 4: <0.0001(***)	z = -10.8868
													3 vs 4: 0.0001(***)	z = -4.2601
3E	Duration	5	cluster 0 (n=48)	cluster 1 (n=54)	cluster 2 (n=121)	cluster 3 (n=94)	cluster 4 (n=64)	clusters	Kruskal-Wallis test	<0.0001(***)	32.71	Dunn's test	0 vs 1: 0.0035(**)	z = 3.3877
													0 vs 2: <0.0001(***)	z = 4.3376
													1 vs 2: 1(ns)	z = 0.4147
													0 vs 3: <0.0001(***)	z = 4.6324
													1 vs 3: 1(ns)	z = 0.8771
													2 vs 3: 1(ns)	z = 0.5956
													0 vs 4: 1(ns)	z = 1.2402
													1 vs 4: 0.0925(ns)	z = -2.3553
													2 vs 4: 0.0057(**)	z = -3.2549
													3 vs 4: 0.0015(**)	z = -3.6096
3E	Depth	5	cluster 0 (n=48)	cluster 1 (n=54)	cluster 2 (n=121)	cluster 3 (n=94)	cluster 4 (n=64)	clusters	Kruskal-Wallis test	<0.0001(***)	236.67	Dunn's test	0 vs 1: 1(ns)	z = -0.8047
													0 vs 2: <0.0001(***)	z = -7.0018
													1 vs 2: <0.0001(***)	z = -6.3227
													0 vs 3: <0.0001(***)	z = -11.816
													1 vs 3: <0.0001(***)	z = -11.3412
													2 vs 3: <0.0001(***)	z = -6.5593
													0 vs 4: <0.0001(***)	z = -10.1204
													1 vs 4: <0.0001(***)	z = -9.5939
													2 vs 4: <0.0001(***)	z = -4.7749
													3 vs 4: 1(ns)	z = 1.0107
4D	Duration	4	cluster 1 (n=584)	cluster 1 (n=170)	cluster 2 (n=1080)	cluster 3 (n=29)		clusters	Kruskal-Wallis test	<0.0001(***)	119.53	Dunn's test	0 vs 1: 0.0311(*)	z = -2.5631
													0 vs 2: <0.0001(***)	z = -2.5631
													1 vs 2: 0.0007(***)	z = -3.6737
													0 vs 3: 0.2611(ns)	z = 1.7113
													1 vs 3: 0.0189(*)	z = 2.7323
													2 vs 3: <0.0001(***)	z = 4.5281
4D	Directedness	4	cluster 1 (n=584)	cluster 1 (n=170)	cluster 2 (n=1080)	cluster 3 (n=29)		clusters	Kruskal-Wallis test	<0.0001(***)	70.77	Dunn's test	0 vs 1: 0.022(*)	z = 2.6812
													0 vs 2: <0.0001(***)	z = 2.6812
													1 vs 2: 0.0507(ns)	z = 2.3889
													0 vs 3: 0.2251(ns)	z = 1.7802
													1 vs 3: 1(ns)	z = 0.5228
													2 vs 3: 1(ns)	z = -0.4894
4H	Duration	4	cluster 0 (n=335)	cluster 1 (n=927)	cluster 2 (n=806)	cluster 3 (n=222)		clusters	Kruskal-Wallis test	<0.0001(***)	115.97	Dunn's test	0 vs 1: <0.0001(***)	z = -4.3936
													0 vs 2: 0.1178(ns)	z = -4.3936
													1 vs 2: <0.0001(***)	z = 8.5979
													0 vs 3: <0.0001(***)	z = 4.3073
													1 vs 3: <0.0001(***)	z = 8.7371
													2 vs 3: 0.0049(**)	z = 3.1501
4H	Directedness	4	cluster 0 (n=335)	cluster 1 (n=927)	cluster 2 (n=806)	cluster 3 (n=222)		clusters	Kruskal-Wallis test	<0.0001(***)	89.86	Dunn's test	0 vs 1: 0.1394(ns)	z = -1.9912
													0 vs 2: <0.0001(***)	z = -1.9912
													1 vs 2: <0.0001(***)	z = -5.0746
													0 vs 3: <0.0001(***)	z = -7.9756
													1 vs 3: <0.0001(***)	z = -7.5386
													2 vs 3: <0.0001(***)	z = -4.2072
	Parameter	Number of Groups	Group 1	Group 2	Group 3	Group 4	Group 5	Unit of number	Statistical tests used	p value of multiple test	Other result of multiple test	Post-hoc test	p value of post-hoc test	Other result of post-hoc test
	Avoidance distance	3	naive (n=50)	mock (n=50)	preexp. (n=50)				Kruskal-Wallis test	<0.0001(***)	24.451	Dunn's test	naive vs mock: 0.7621(ns)	z = 0.6619
													naive vs preexp.: <0.0001(***)	z = 4.5747
													mock vs preexp.: 0.0001(***)	z = 3.9128
	Cluster 0 duration	3	naive (n=347)	mock (n=373)	preexp. (n=349)				Kruskal-Wallis test		29.20	Dunn's test	naive vs mock: 1(ns)	z = -0.1812
													naive vs preexp.: <0.0001(***)	z = -4.739
													mock vs preexp.: <0.0001(***)	z = -4.6426
	Initial velocity	3	naive (n=347)	mock (n=373)	preexp. (n=349)				Kruskal-Wallis test			Dunn's test	naive vs mock: <0.0001(***)	z = 5.2709
													naive vs preexp.: <0.0001(***)	z = 9.3668
													mock vs preexp.: <0.0001(***)	z = 4.2561

Figure	Parameter	Number of Groups	Group 1	Group 2	Group 3	Group 4	Group 5	Unit of number	Statistical tests used	p value of multiple test	Other result of multiple test	Post-hoc test	p value of post-hoc test	Other result of post-hoc test
	Duration	4	cluster 0 (n=335)	cluster 1 (n=927)	cluster 2 (n=806)	cluster 3 (n=222)			Kruskal-Wallis test		115.97	Dunn's test	0 vs 1: <0.0001(***) 0 vs 2: 0.1178(ns) 1 vs 2: <0.0001(***) 0 vs 3: <0.0001(***) 1 vs 3: <0.0001(***) 2 vs 3: 0.0049(**)	z = -4.3936 z = -4.3936 z = 8.5979 z = 4.3073 z = 8.7371 z = 3.1501
6A	Avoidance distance	3	naive (n=50)	mock (n=50)	preexp. (n=50)			animals	Kruskal-Wallis test	<0.0001(***)	24.451	Dunn's test	naive vs mock: 0.7621(ns) naive vs preexp.: <0.0001(***) mock vs preexp.: 0.0001(***)	z = 0.6619 z = 4.5747 z = 3.9128
6B	Cluster 0 duration	3	naive (n=347)	mock (n=373)	preexp. (n=349)			clusters	Kruskal-Wallis test	<0.0001(***)	29.20	Dunn's test	naive vs mock: 1(ns) naive vs preexp.: <0.0001(***) mock vs preexp.: <0.0001(***)	z = -0.1812 z = -4.739 z = -4.6426
6C	Initial velocity	3	naive (n=347)	mock (n=373)	preexp. (n=349)			clusters	Kruskal-Wallis test	<0.0001(***)	88.07	Dunn's test	naive vs mock: <0.0001(***) naive vs preexp.: <0.0001(***) mock vs preexp.: <0.0001(***)	z = 5.2709 z = 9.3668 z = 4.2561
6D	Average concentration	3	naive (n=347)	mock (n=373)	preexp. (n=349)			clusters	Kruskal-Wallis test	<0.0001(***)	85.60	Dunn's test	naive vs mock: 1(ns) naive vs preexp.: <0.0001(***) mock vs preexp.: <0.0001(***)	z = -0.3344 z = 7.7844 z = 8.259
6E	Averege of concentration change	3	naive (n=347)	mock (n=373)	preexp. (n=349)			clusters	Kruskal-Wallis test	0.0003(***)	48.83	Dunn's test	naive vs mock: 0.24(ns) naive vs preexp.: <0.0001(***) mock vs preexp.: <0.0001(***)	z = -1.405 z = -6.6052 z = -5.3166
7C	Peak value of GCaMP3/mCherry	3	naive (n=25)	mock (n=29)	preexp. (n=28)			animals	Kruskal-Wallis test	<0.0001(***)	30.11	Dunn's test	naive vs mock: 0.0949(ns) naive vs preexp.: <0.0001(***) mock vs preexp.: 0.0004(***)	z = 1.8571 z = 5.3589 z = 3.6525
9D	Fight velocity in 3D space at t=-0.3	2	initial (n=27)	last (n=27)				flights	Mann–Whitney test	0.0234(*)	233.000	-	-	-
9D	Flight acceleration in 3D space at t=-0.3	2	initial (n=27)	last (n=27)				flights	Mann–Whitney test	0.2326(ns)	295.00	-	-	-
S2D	Velocity	5	cluster 0 (n=97)	cluster 1 (n=112)	cluster 2 (n=117)	cluster 3 (n=30)	cluster 4 (n=9)	clusters	Kruskal-Wallis test	<0.0001(***)	224.45	Dunn's test	0 vs 1: 0.0034(**) 0 vs 2: <0.0001(***) 1 vs 2: <0.0001(***) 0 vs 3: <0.0001(***) 1 vs 3: <0.0001(***) 2 vs 3: 0.0632(ns) 0 vs 4: <0.0001(***) 1 vs 4: <0.0001(***) 2 vs 4: 0.1187(ns) 3 vs 4: 1(ns)	z = -3.3957 z = -11.7674 z = -8.6606 z = -10.178 z = -8.0519 z = -2.494 z = -6.882 z = -5.5621 z = -2.2612 z = -0.7152
S2D	Duration	5	cluster 0 (n=97)	cluster 1 (n=112)	cluster 2 (n=117)	cluster 3 (n=30)	cluster 4 (n=9)	clusters	Kruskal-Wallis test	<0.0001(***)	51.09	Dunn's test	0 vs 1: 0.0072(**) 0 vs 2: 0.6346(ns) 1 vs 2: <0.0001(***) 0 vs 3: 0.0001(***) 1 vs 3: 0.172(ns) 2 vs 3: <0.0001(***) 0 vs 4: 0.0063(**) 1 vs 4: 0.2455(ns) 2 vs 4: 0.0006(***) 3 vs 4: 1(ns)	z = 3.1845 z = -1.5264 z = -4.9268 z = 4.1959 z = 2.1153 z = 5.3074 z = 3.2241 z = 1.9677 z = 3.8537 z = 0.6496
S2D	Depth	5	cluster 0 (n=97)	cluster 1 (n=112)	cluster 2 (n=117)	cluster 3 (n=30)	cluster 4 (n=9)	clusters	Kruskal-Wallis test	<0.0001(***)	197.3806	Dunn's test	0 vs 1: 0.9449(ns) 0 vs 2: <0.0001(***) 1 vs 2: <0.0001(***) 0 vs 3: <0.0001(***) 1 vs 3: <0.0001(***) 2 vs 3: 0.6961(ns) 0 vs 4: <0.0001(***) 1 vs 4: <0.0001(***) 2 vs 4: 1(ns) 3 vs 4: 1(ns)	z = -1.3136 z = -10.8527 z = -9.895 z = -8.5822 z = -7.835 z = -1.4787 z = -5.2045 z = -4.7085 z = -0.9345 z = -0.0543

Supplementary Table 2. Information gains for wild-type.

time	value	Clst0Dur	Clst1Dur	V				dV				B				dB				Dir				C				dC				WV
		All	All	All	Ini	Mid	Ter	All	Ini	Mid	Ter	All	Ini	Mid	Ter	All	Ini	Mid	Ter	All	Ini	Mid	Ter	All	Ini	Mid	Ter	All	Ini	Mid	Ter	All
-	Ave	0.0975	0.0569	-	-	-	-	-	-	-	-	-	-	-	-	0.0715	-	-	-	-	-	-	-	0.1633	-	-	-	0.0879	-	-	-	-
-	Med	-	-	0.0401	-	-	-	-	-	-	-	-	-	-	-	0.1017	-	-	-	-	-	-	-	0.1603	-	-	-	0.0883	-	-	-	-
-	Q1st	-	-	-	-	-	-	-	-	-	-	-	-	-	-	0.0645	-	-	-	-	-	-	-	0.1635	-	-	-	0.1072	-	-	-	-
-	Q3rd	-	-	-	-	-	-	-	-	-	-	-	-	-	-	0.0828	-	-	-	-	-	-	-	0.1605	-	-	-	0.0799	-	-	-	-
-	Var	-	-	-	-	-	-	-	-	-	-	-	-	-	-	-	-	-	-	-	-	-	-	-	-	-	-	0.0797	-	-	-	-
-	1 %ile	-	-	-	-	-	-	-	-	-	-	-	-	-	-	-	-	-	-	-	-	-	-	0.1634	-	-	-	0.0904	-	-	-	-
-	5 %ile	-	-	-	-	-	-	-	-	-	-	-	-	-	-	-	-	-	-	-	-	-	-	0.1645	-	-	-	0.0998	-	-	-	-
-	95 %ile	-	-	-	-	-	-	-	-	-	-	-	-	-	-	-	-	-	-	-	-	-	-	0.1532	-	-	-	0.1078	-	-	-	-
-	99 %ile	-	-	-	-	-	-	-	-	-	-	-	-	-	-	-	-	-	-	-	-	-	-	0.1482	-	-	-	0.0601	-	-	-	-
1	Ave	-	-	-	0.1137	-	-	-	-	-	-	-	-	-	-	-	-	-	-	-	-	-	-	-	0.1471	0.162	0.162	-	0.1163	0.0927	0.1043	-
2	Ave	-	-	-	0.1203	-	0.049	-	-	-	-	-	-	-	-	-	-	0.0478	-	-	-	-	-	-	0.1478	0.1655	0.163	-	0.1107	0.1048	0.1219	-
3	Ave	-	-	-	0.1088	-	-	-	-	-	-	-	-	-	-	-	-	0.0487	-	-	-	-	-	-	0.1508	0.1633	0.1621	-	0.1096	0.0986	0.1277	-
3	Med	-	-	-	0.0996	-	0.0391	-	-	-	-	-	-	-	-	-	-	-	-	-	-	-	-	-	0.1491	0.162	0.1622	-	0.114	0.0894	0.1338	-
3	Var	-	-	-	-	-	-	-	-	-	-	-	-	-	-	-	-	-	-	-	-	-	-	-	0.1114	0.0866	0.0408	-	0.0596	0.0504	-	-
4	Ave	-	-	-	0.0987	-	-	-	-	-	-	-	-	-	-	-	-	0.0504	-	-	-	-	-	-	0.1465	0.1655	0.1654	-	0.082	0.0984	0.1218	-
4	Med	-	-	-	0.0999	-	-	-	-	-	-	-	-	-	-	-	-	-	-	-	-	-	-	-	0.1486	0.1655	0.1647	-	0.0853	0.0965	0.1447	-
4	Var	-	-	-	-	-	-	-	-	-	-	-	-	-	-	-	-	-	-	-	-	-	-	-	0.1024	0.083	0.0402	-	0.0572	0.0821	0.0817	-
5	Ave	-	-	-	-	-	-	-	-	-	-	-	-	-	-	-	-	0.0483	-	-	-	-	-	-	0.1458	0.1633	0.166	-	0.0903	0.1117	0.148	-
5	Med	-	-	-	0.0778	-	-	-	-	-	-	-	-	-	-	-	-	-	-	-	-	-	-	-	0.148	0.162	0.1653	-	0.0926	0.1104	0.1248	-
5	Var	-	-	-	-	-	-	-	-	-	-	-	-	-	-	-	-	-	-	-	-	-	-	-	0.0968	0.092	0.0537	-	0.0609	0.1124	0.0782	-
6	Ave	-	-	-	0.0718	-	-	-	-	-	-	-	-	-	-	-	-	0.0562	-	-	-	-	-	-	0.1477	0.1642	0.1459	-	0.0833	0.1117	0.1686	-
6	Med	-	-	-	0.0747	-	-	-	-	-	-	-	-	-	-	-	-	-	-	-	-	-	-	-	0.148	0.1655	0.1466	-	0.085	0.1111	0.1489	-
6	Var	-	-	-	-	-	-	-	-	-	-	-	-	-	-	-	-	-	-	-	-	-	-	-	0.089	0.0953	0.0601	-	-	0.1162	0.081	-

Supplementary Table 3. Information gains for *egl-3(n589)*.

time	value	Clst0Dur All	Clst1Dur All	V All	V Ini	V Mid	V Ter	dV All	dV Ini	dV Mid	dV Ter	B All	B Ini	B Mid	B Ter	dB All	dB Ini	dB Mid	dB Ter	Dir All	Dir Ini	Dir Mid	Dir Ter	C All	C Ini	C Mid	C Ter	dC All	dC Ini	dC Mid	dC Ter	WV All
-	Ave			-	-	-	-	-	-	-	-	-	-	-	-	-	-	-	-	-	-	-	-	0.1179	-	-	-	-	-	-	-	-
-	Med	-	-	-	-	-	-	-	-	-	-	-	-	-	-	-	-	-	-	-	-	-	-	0.1179	-	-	-	-	-	-	-	-
-	Q1st	-	-	-	-	-	-	-	-	-	-	-	-	-	-	-	-	-	-	-	-	-	-	0.1209	-	-	-	-	-	-	-	-
-	Q3rd	-	-	-	-	-	-	-	-	-	-	-	-	-	-	-	-	-	-	-	-	-	-	0.1191	-	-	-	-	-	-	-	-
-	Var	-	-	-	-	-	-	-	-	-	-	-	-	-	-	-	-	-	-	-	-	-	-		-	-	-	-	-	-	-	-
-	1 %ile	-	-	-	-	-	-	-	-	-	-	-	-	-	-	-	-	-	-	-	-	-	-	0.1138	-	-	-	-	-	-	-	-
-	5 %ile	-	-	-	-	-	-	-	-	-	-	-	-	-	-	-	-	-	-	-	-	-	-	0.1138	-	-	-	-	-	-	-	-
-	95 %ile	-	-	-	-	-	-	-	-	-	-	-	-	-	-	-	-	-	-	-	-	-	-	0.1396	-	-	-	-	-	-	-	-
-	99 %ile	-	-	-	-	-	-	-	-	-	-	-	-	-	-	-	-	-	-	-	-	-	-	0.1485	-	-	-	-	-	-	-	-
1	Ave	-	-	-				-				-				-				-				-	0.1416	0.1163	0.1233	-				-
2	Ave	-	-	-				-				-				-				-				-	0.146	0.1163	0.1251	-				-
3	Ave	-	-	-				-				-				-				-				-	0.1489	0.1163	0.1209	-				-
3	Med	-	-	-				-				-				-				-	-	-	-	-	0.146	0.1163	0.1251	-				-
3	Var	-	-	-				-				-				-				-	-	-	-	-				-				-
4	Ave	-	-	-				-				-				-				-				-	0.1402	0.1163	0.1209	-				-
4	Med	-	-	-				-				-				-				-	-	-	-	-	0.146	0.1163	0.1209	-				-
4	Var	-	-	-				-				-				-				-	-	-	-	-				-				-
5	Ave	-	-	-				-				-				-				-				-	0.1402	0.1163	0.1209	-				-
5	Med	-	-	-				-				-				-				-	-	-	-	-	0.1402	0.1163	0.1191	-				-
5	Var	-	-	-				-				-				-				-	-	-	-	-				-				-
6	Ave	-	-	-				-				-				-				-				-	0.1398	0.1163	0.1251	-				-
6	Med	-	-	-				-				-				-				-	-	-	-	-	0.1398	0.1163	0.1191	-				-
6	Var	-	-	-				-				-				-				-	-	-	-	-				-				-

Supplementary Table 4. Information gains for *egl-3(ok979)*.

time	value	Clst0Dur All	Clst1Dur All	V All	V Ini	V Mid	V Ter	dV All	dV Ini	dV Mid	dV Ter	B All	B Ini	B Mid	B Ter	dB All	dB Ini	dB Mid	dB Ter	Dir All	Dir Ini	Dir Mid	Dir Ter	C All	C Ini	C Mid	C Ter	dC All	dC Ini	dC Mid	dC Ter	WV All
-	Ave	-	-	0.5665	-	-	-	-	-	-	-	-	-	-	-	-	-	-	-	-	-	-	-	0.1766	-	-	-	-	-	-	-	-
-	Med	-	-	0.4535	-	-	-	-	-	-	-	-	-	-	-	-	-	-	-	-	-	-	-	0.1821	-	-	-	-	-	-	-	-
-	Q1st	-	-	0.3885	-	-	-	-	-	-	-	-	-	-	-	-	-	-	-	-	-	-	-	0.1772	-	-	-	-	-	-	-	-
-	Q3rd	-	-	0.531	-	-	-	-	-	-	-	-	-	-	-	-	-	-	-	-	-	-	-	0.1703	-	-	-	-	-	-	-	-
-	Var	-	-	-	-	-	-	-	-	-	-	-	-	-	-	-	-	-	-	-	-	-	-	-	-	-	-	-	-	-	-	-
-	1 %ile	-	-	-	-	-	-	-	-	-	-	-	-	-	-	-	-	-	-	-	-	-	-	0.187	-	-	-	-	-	-	-	-
-	5 %ile	-	-	-	-	-	-	-	-	-	-	-	-	-	-	-	-	-	-	-	-	-	-	0.187	-	-	-	-	-	-	-	-
-	95 %ile	-	-	0.4334	-	-	-	-	-	-	-	-	-	-	-	-	-	-	-	-	-	-	-	0.1611	-	-	-	-	-	-	-	-
-	99 %ile	-	-	0.4201	-	-	-	-	-	-	-	-	-	-	-	-	-	-	-	-	-	-	-	0.1611	-	-	-	-	-	-	-	-
1	Ave	-	-	-	0.153	0.2297		-				-				-				-				-	0.172	0.1821	0.1727	-				-
2	Ave	-	-	-	0.1977	0.2102		-				-				-				-				-	0.172	0.1821	0.1727	-				-
3	Ave	-	-	-	0.2585	0.3037	0.2213	-				-				-				-				-	0.1737	0.1821	0.1727	-				-
3	Med	-	-	-	0.2252	0.2769	0.2474	-				-				-				-				-	0.1727	0.1821	0.1727	-				-
3	Var	-	-	-				-				-				-			-	-			-	-				-				-
4	Ave	-	-	-	0.2805	0.3375	0.3015	-				-				-				-				-	0.1737	0.1821	0.1727	-				-
4	Med	-	-	-	0.2502	0.351	0.3091	-				-				-				-			-	-	0.1737	0.1821	0.1727	-				-
4	Var	-	-	-				-				-				-				-				-	-				-				-
5	Ave	-	-	-	0.2821	0.3142	0.3748	-				-				-				-				-	0.1737	0.1821	0.1727	-				-
5	Med	-	-	-	0.3144	0.3859	0.3277	-				-				-				-				-	0.1737	0.1821	0.1727	-				-
5	Var	-	-	-				-	0.1696			-				-			-	-				-	-				-				-
6	Ave	-	-	-	0.3166	0.3806	0.4495	-				-				-				-				-	0.1727	0.1821	0.1727	-				-
6	Med	-	-	-	0.3362	0.3934	0.4197	-				-				-				-				-	0.1737	0.1821	0.1727	-				-
6	Var	-	-	-				-	0.1814			-				-				-			-	-	-				-				-

Supplementary Table 5. Information gains for *egl-21*.

time	value	Clst0Dur	Clst1Dur	V				dV				B				dB				Dir				C				dC				WV
		All	All	All	Ini	Mid	Ter	All	Ini	Mid	Ter	All	Ini	Mid	Ter	All	Ini	Mid	Ter	All	Ini	Mid	Ter	All	Ini	Mid	Ter	All	Ini	Mid	Ter	All
-	Ave			-	-	-		-	-	-		-	-	-		-	-	-		-	-	-		-	-	-		-	-	-		
-	Med	-	-	-	-	-	-	-	-	-	-	-	-	-	-	-	-	-	-	-	-	-	-	-	-	-	-	-	-	-	-	-
-	Q1st	-	-	-	-	-	-	-	-	-	-	-	-	-	-	-	-	-	-	-	-	-	-	-	-	-	-	-	-	-	-	-
-	Q3rd	-	-	-	-	-	-	-	-	-	-	-	-	-	-	-	-	-	-	-	-	-	-	-	-	-	-	-	-	-	-	-
-	Var	-	-	-	-	-	-	-	-	-	-	-	-	-	-	-	-	-	-	-	-	-	-	-	-	-	-	-	-	-	-	-
-	1 %ile	-	-	-	-	-	-	-	-	-	-	-	-	-	-	-	-	-	-	-	-	-	-	-	-	-	-	-	-	-	-	-
-	5 %ile	-	-	-	-	-	-	-	-	-	-	-	-	-	-	-	-	-	-	-	-	-	-	-	-	-	-	-	-	-	-	-
-	95 %ile	-	-	-	-	-	-	-	-	-	-	-	-	-	-	-	-	-	-	-	-	-	-	-	-	-	-	-	-	-	-	-
-	99 %ile	-	-	-	-	-	-	-	-	-	-	-	-	-	-	-	-	-	-	-	-	-	-	-	-	-	-	-	-	-	-	-
1	Ave	-	-	-				-				-				-				-				-				-				-
2	Ave	-	-	-				-				-				-				-				-				-				-
3	Ave	-	-	-				-				-				-				-				-				-				-
3	Med	-	-	-				-				-				-				-	-	-	-	-				-				-
3	Var	-	-	-				-				-				-				-	-	-	-	-				-				-
4	Ave	-	-	-				-				-				-				-				-				-				-
4	Med	-	-	-				-				-				-				-	-	-	-	-				-				-
4	Var	-	-	-				-				-				-				-	-	-	-	-				-				-
5	Ave	-	-	-				-				-				-				-				-				-				-
5	Med	-	-	-				-				-				-				-	-	-	-	-				-				-
5	Var	-	-	-				-				-				-				-	-	-	-	-				-				-
6	Ave	-	-	-				-				-				-				-				-				-				-
6	Med	-	-	-				-				-				-				-	-	-	-	-				-				-
6	Var	-	-	-				-				-				-				-	-	-	-	-				-				-

Supplementary Table 6. Information gains for *dop-3*.

time	value	Clst0Dur	Clst1Dur	V				dV				B				dB				Dir				C				dC				WV
		All	All	All	Ini	Mid	Ter	All	Ini	Mid	Ter	All	Ini	Mid	Ter	All	Ini	Mid	Ter	All	Ini	Mid	Ter	All	Ini	Mid	Ter	All	Ini	Mid	Ter	All
-	Ave	0.0682	-	0.1111	-	-	-	-	-	-	-	0.1133	-	-	-	-	-	-	-	0.0997	-	-	-	-	-	-	-	0.1233	-	-	-	-
-	Med	-	-	0.1138	-	-	-	-	-	-	-	0.092	-	-	-	-	-	-	-	-	-	-	-	-	-	-	-	0.1467	-	-	-	-
-	Q1st	-	-	0.1152	-	-	-	-	-	-	-	0.059	-	-	-	-	-	-	-	-	-	-	-	-	-	-	-	-	-	-	-	-
-	Q3rd	-	-	0.083	-	-	-	-	-	-	-	0.1097	-	-	-	-	-	-	-	-	-	-	-	-	-	-	-	0.1197	-	-	-	-
-	Var	-	-	-	-	-	-	-	-	-	-	0.0891	-	-	-	-	-	-	-	-	-	-	-	-	-	-	-	0.0787	-	-	-	-
-	1 %ile	-	-	0.0489	-	-	-	-	-	-	-	-	-	-	-	-	-	-	-	-	-	-	-	-	-	-	-	-	-	-	-	-
-	5 %ile	-	-	0.0603	-	-	-	-	-	-	-	-	-	-	-	-	-	-	-	-	-	-	-	-	-	-	-	-	-	-	-	-
-	95 %ile	-	-	0.0573	-	-	-	-	-	-	-	0.119	-	-	-	-	-	-	-	-	-	-	-	-	-	-	-	0.1146	-	-	-	-
-	99 %ile	-	-	-	-	-	-	-	-	-	-	0.1378	-	-	-	-	-	-	-	-	-	-	-	-	-	-	-	0.1168	-	-	-	-
1	Ave	-	-	-	-	0.0538	0.0462	-	-	0.0504	0.0978	-	-	-	-	-	-	-	-	-	-	-	-	-	-	-	-	-	-	-	0.1226	-
2	Ave	-	-	-	-	0.068	0.0889	-	-	-	-	-	-	-	0.1119	-	-	-	-	-	-	-	-	-	-	-	-	-	-	0.0793	0.1532	-
3	Ave	-	-	-	-	0.0722	0.1143	-	-	-	-	-	-	-	0.1261	-	-	-	0.0467	-	-	-	-	-	-	-	-	-	-	0.0947	0.1548	-
3	Med	-	-	-	-	0.0547	0.1581	-	-	-	-	-	-	-	0.1397	-	-	-	-	-	-	-	-	-	-	-	-	-	-	0.0879	0.1721	-
3	Var	-	-	-	-	-	-	-	-	-	-	-	-	-	-	-	-	-	-	-	-	-	-	-	-	-	-	-	-	-	-	-
4	Ave	-	-	-	-	0.0557	0.1373	-	-	0.0444	0.1353	-	-	-	-	-	-	-	-	-	-	-	-	-	-	-	-	-	-	0.0958	0.1585	-
4	Med	-	-	-	-	0.0601	0.1264	-	-	-	-	-	-	-	0.139	-	-	-	-	-	-	-	-	-	-	-	-	-	-	0.0919	0.1674	-
4	Var	-	-	-	-	-	-	-	-	-	-	-	-	-	-	-	-	-	-	-	-	-	-	-	-	-	-	-	-	-	-	-
5	Ave	-	-	-	-	0.0516	0.1365	-	-	-	-	-	-	-	0.1326	-	-	-	0.0513	-	-	-	-	-	-	-	-	-	-	0.103	0.1613	-
5	Med	-	-	-	-	0.0702	0.1162	-	-	-	-	-	-	-	0.1274	-	-	-	-	-	-	-	-	-	-	-	-	-	-	0.0979	0.1549	-
5	Var	-	-	-	-	-	-	-	-	-	-	-	-	-	0.0614	-	-	-	0.0488	-	-	-	-	-	-	-	-	-	-	-	-	-
6	Ave	-	-	-	-	0.0592	0.1514	-	-	-	-	-	-	-	0.1314	-	-	-	-	-	-	-	0.0527	-	-	-	-	-	-	0.1164	0.1632	-
6	Med	-	-	-	-	0.059	0.1383	-	-	-	-	-	-	-	0.1288	-	-	-	-	-	-	-	-	-	-	-	-	-	-	0.0929	0.1537	-
6	Var	-	-	-	-	-	-	-	-	-	-	-	-	-	0.0681	-	-	-	0.0678	-	-	-	-	-	-	-	-	-	-	-	-	-

Supplementary Table 7. Information gains for *ocr-2*.

time	value	Clst0Dur All	Clst1Dur All	V All	V Ini	V Mid	V Ter	dV All	dV Ini	dV Mid	dV Ter	B All	B Ini	B Mid	B Ter	dB All	dB Ini	dB Mid	dB Ter	Dir All	Dir Ini	Dir Mid	Dir Ter	C All	C Ini	C Mid	C Ter	dC All	dC Ini	dC Mid	dC Ter	WV All
-	Ave		-	0.1229	-	-	-	-	-	-	-	-	-	-	-	-	-	-	-	-	-	-	-	-	-	-	-	-	-	-	-	-
-	Med	-	-	0.1362	-	-	-	-	-	-	-	-	-	-	-	-	-	-	-	-	-	-	-	-	-	-	-	-	-	-	-	-
-	Q1st	-	-	0.1412	-	-	-	-	-	-	-	-	-	-	-	-	-	-	-	-	-	-	-	-	-	-	-	-	-	-	-	-
-	Q3rd	-	-	0.1226	-	-	-	-	-	-	-	-	-	-	-	-	-	-	-	-	-	-	-	-	-	-	-	-	-	-	-	-
-	Var	-	-	-	-	-	-	-	-	-	-	-	-	-	-	-	-	-	-	-	-	-	-	-	-	-	-	-	-	-	-	-
-	1 %ile	-	-	-	-	-	-	-	-	-	-	-	-	-	-	-	-	-	-	-	-	-	-	-	-	-	-	-	-	-	-	-
-	5 %ile	-	-	-	-	-	-	-	-	-	-	-	-	-	-	-	-	-	-	-	-	-	-	-	-	-	-	-	-	-	-	-
-	95 %ile	-	-	-	-	-	-	-	-	-	-	-	-	-	-	-	-	-	-	-	-	-	-	-	-	-	-	-	-	-	-	-
-	99 %ile	-	-	-	-	-	-	-	-	-	-	-	-	-	-	-	-	-	-	-	-	-	-	-	-	-	-	-	-	-	-	-
1	Ave	-	-	-				-				-				-				-				-				-				-
2	Ave	-	-	-				-				-				-				-				-				-				-
3	Ave	-	-	-				-				-				-				-				-				-				-
3	Med	-	-	-			0.1	-				-				-				-	-	-	-	-				-				-
3	Var	-	-	-				-				-				-				-	-	-	-	-				-				-
4	Ave	-	-	-				-				-				-				-				-				-				-
4	Med	-	-	-			0.1051	-				-				-				-	-	-	-	-				-				-
4	Var	-	-	-				-				-				-				-	-	-	-	-				-				-
5	Ave	-	-	-			0.1663	-				-				-				-				-				-				-
5	Med	-	-	-			0.1657	-				-				-				-	-	-	-	-				-				-
5	Var	-	-	-				-				-				-				-	-	-	-	-				-				-
6	Ave	-	-	-			0.1086	-				-				-				-				-				-				-
6	Med	-	-	-			0.1474	-				-				-				-	-	-	-	-				-				-
6	Var	-	-	-				-				-				-				-	-	-	-	-				-				-

Supplementary Table 8. Information gains for *osm-9*.

time	value	Clst0Dur All	Clst1Dur All	V All	V Ini	V Mid	V Ter	dV All	dV Ini	dV Mid	dV Ter	B All	B Ini	B Mid	B Ter	dB All	dB Ini	dB Mid	dB Ter	Dir All	Dir Ini	Dir Mid	Dir Ter	C All	C Ini	C Mid	C Ter	dC All	dC Ini	dC Mid	dC Ter	WV All
-	Ave	0.0963	-	0.2378	-	-	-	-	-	-	-	-	-	-	-	-	-	-	-	-	-	-	-	-	-	-	-	-	-	-	-	-
-	Med	-	-	0.2247	-	-	-	-	-	-	-	-	-	-	-	-	-	-	-	-	-	-	-	-	-	-	-	-	-	-	-	-
-	Q1st	-	-	0.2555	-	-	-	-	-	-	-	-	-	-	-	-	-	-	-	-	-	-	-	-	-	-	-	-	-	-	-	-
-	Q3rd	-	-	0.1996	-	-	-	-	-	-	-	-	-	-	-	-	-	-	-	-	-	-	-	-	-	-	-	-	-	-	-	-
-	Var	-	-	-	-	-	-	-	-	-	-	-	-	-	-	-	-	-	-	-	-	-	-	0.1101	-	-	-	-	-	-	-	-
-	1 %ile	-	-	-	-	-	-	-	-	-	-	-	-	-	-	-	-	-	-	-	-	-	-	-	-	-	-	-	-	-	-	-
-	5 %ile	-	-	-	-	-	-	-	-	-	-	-	-	-	-	-	-	-	-	-	-	-	-	-	-	-	-	-	-	-	-	-
-	95 %ile	-	-	0.1553	-	-	-	-	-	-	-	-	-	-	-	-	-	-	-	-	-	-	-	-	-	-	-	-	-	-	-	-
-	99 %ile	-	-	0.1249	-	-	-	-	-	-	-	-	-	-	-	-	-	-	-	-	-	-	-	-	-	-	-	-	-	-	-	-
1	Ave	-	-	-				-				-				-				-				-				-				-
2	Ave	-	-	-		0.1382		-				-				-				-				-				-				-
3	Ave	-	-	-		0.1437		-				-				-				-				-				-				-
3	Med	-	-	-		0.1558	0.0922	-				-				-				-	-	-	-	-				-				-
3	Var	-	-	-				-				-				-				-	-	-	-	-				-				-
4	Ave	-	-	-		0.1433		-				-				-				-				-				-				-
4	Med	-	-	-		0.1641		-				-				-				-	-	-	-	-				-				-
4	Var	-	-	-				-				-				-				-	-	-	-	-				-				-
5	Ave	-	-	-	0.0724	0.1637		-				-				-				-				-				-				-
5	Med	-	-	-	0.0859	0.1597	0.1115	-				-				-				-	-	-	-	-				-				-
5	Var	-	-	-				-				-				-				-	-	-	-	-				-				-
6	Ave	-	-	-	0.0884	0.1872	0.1012	-				-				-				-				-				-				-
6	Med	-	-	-	0.1197	0.1735	0.1116	-				-				-				-	-	-	-	-				-				-
6	Var	-	-	-				-				-				-				-	-	-	-	-				-				-

Supplementary Table 9. Information gains for *tax-4*.

time	value	Clst0Dur	Clst1Dur	V				dV				B				dB				Dir				C				dC				WV
		All	All	All	Ini	Mid	Ter	All	Ini	Mid	Ter	All	Ini	Mid	Ter	All	Ini	Mid	Ter	All	Ini	Mid	Ter	All	Ini	Mid	Ter	All	Ini	Mid	Ter	All
-	Ave				-	-	-		-	-	-		-	-	-		-	-	-		-	-	-	0.2677	-	-	-		-	-	-	-
-	Med	-	-		-	-	-		-	-	-		-	-	-		-	-	-		-	-	-	0.268	-	-	-		-	-	-	-
-	Q1st	-	-		-	-	-		-	-	-		-	-	-		-	-	-		-	-	-	0.232	-	-	-		-	-	-	-
-	Q3rd	-	-		-	-	-		-	-	-		-	-	-		-	-	-		-	-	-	0.2832	-	-	-		-	-	-	-
-	Var	-	-		-	-	-		-	-	-		-	-	-		-	-	-		-	-	-		-	-	-		-	-	-	-
-	1 %ile	-	-		-	-	-		-	-	-		-	-	-	0.0739	-	-	-		-	-	-	0.2412	-	-	-		-	-	-	-
-	5 %ile	-	-		-	-	-		-	-	-		-	-	-		-	-	-		-	-	-	0.2387	-	-	-		-	-	-	-
-	95 %ile	-	-		-	-	-		-	-	-		-	-	-		-	-	-		-	-	-	0.2825	-	-	-		-	-	-	-
-	99 %ile	-	-		-	-	-		-	-	-		-	-	-		-	-	-		-	-	-	0.2776	-	-	-		-	-	-	-
1	Ave	-	-	-				-				-				-				-				-	0.2324	0.2667	0.2329	-				-
2	Ave	-	-	-				-				-				-				-				-	0.2317	0.2703	0.2329	-				-
3	Ave	-	-	-				-				-				-				-				-	0.2348	0.2667	0.2332	-				-
3	Med	-	-	-		0.1029		-				-				-				-	-	-	-	-	0.2348	0.2667	0.2332	-				-
3	Var	-	-	-				-				-				-				-	-	-	-	-				-				-
4	Ave	-	-	-				-				-				-				-				-	0.2344	0.2703	0.2348	-				-
4	Med	-	-	-				-				-				-				-	-	-	-	-	0.2353	0.2703	0.2332	-				-
4	Var	-	-	-				-				-				-				-	-	-	-	-				-				-
5	Ave	-	-	-				-				-				-	0.0801			-				-	0.2376	0.2671	0.2348	-				-
5	Med	-	-	-				-				-				-	-	-	-	-	-	-	-	-	0.2362	0.2667	0.2348	-				-
5	Var	-	-	-				-				-				-	-	-	-	-	-	-	-	-				-				-
6	Ave	-	-	-				-				-				-				-				-	0.2418	0.271	0.2394	-				-
6	Med	-	-	-				-				-				-	-	-	-	-	-	-	-	-	0.2418	0.2703	0.2394	-				-
6	Var	-	-	-				-				-				-	-	-	-	-	-	-	-	-				-				-

Supplementary Table 10. Information gains for *eat-4*.

time	value	Clst0Dur	Clst1Dur	V				dV				B				dB				Dir				C				dC				WV
		All	All	All	Ini	Mid	Ter	All	Ini	Mid	Ter	All	Ini	Mid	Ter	All	Ini	Mid	Ter	All	Ini	Mid	Ter	All	Ini	Mid	Ter	All	Ini	Mid	Ter	All
-	Ave			0.0905	-	-	-		-	-	-		-	-	-		-	-	-		-	-	-		-	-	-		-	-	-	
-	Med	-	-	0.0922	-	-	-		-	-	-		-	-	-		-	-	-		-	-	-		-	-	-		-	-	-	
-	Q1st	-	-	0.0826	-	-	-		-	-	-		-	-	-		-	-	-		-	-	-		-	-	-		-	-	-	
-	Q3rd	-	-	-	-	-	-		-	-	-		-	-	-		-	-	-		-	-	-		-	-	-		-	-	-	
-	Var	-	-	-	-	-	-		-	-	-		-	-	-		-	-	-		-	-	-		-	-	-		-	-	-	
-	1 %ile	-	-	0.0643	-	-	-		-	-	-		-	-	-		-	-	-		-	-	-		-	-	-		-	-	-	
-	5 %ile	-	-	0.0808	-	-	-		-	-	-		-	-	-		-	-	-		-	-	-		0.0886	-	-	-		-	-	-	
-	95 %ile	-	-	-	-	-	-		-	-	-		-	-	-		-	-	-		-	-	-		-	-	-		-	-	-	
-	99 %ile	-	-	-	-	-	-		-	-	-		-	-	-		-	-	-		-	-	-		-	-	-		-	-	-	
1	Ave	-	-	-	0.0805		0.045	-				-				-				-				-				-				-
2	Ave	-	-	-	0.0834		0.0649	-				-				-				-				-				-				-
3	Ave	-	-	-	0.0866		0.0533	-				-				-				-				-				-				-
3	Med	-	-	-	0.0919		0.065	-				-				-				-	-	-	-	-				-				-
3	Var	-	-	-	-			-				-				-				-	-	-	-	-				-				-
4	Ave	-	-	-	0.0766		0.0505	-				-				-				-				-				-				-
4	Med	-	-	-	0.0771		0.0805	-				-				-				-	-	-	-	-				-				-
4	Var	-	-	-	-			-				-				-				-	-	-	-	-				-				-
5	Ave	-	-	-	0.0955		0.0529	-				-				-				-				-				-				-
5	Med	-	-	-	0.065		0.0493	-				-				-				-	-	-	-	-				-				-
5	Var	-	-	-	-			-				-				-				-	-	-	-	-				-				-
6	Ave	-	-	-	0.0867		0.0481	-				-				-				-				-				-				-
6	Med	-	-	-	0.0634			-				-				-				-	-	-	-	-				-				-
6	Var	-	-	-	-			-				-				-				-	-	-	-	-				-				-

Supplementary Table 11. Information gains for *pkc-1*.

time	value	Clst0Dur	Clst1Dur	V				dV				B				dB				Dir				C				dC				WV
		All	All	All	Ini	Mid	Ter	All	Ini	Mid	Ter	All	Ini	Mid	Ter	All	Ini	Mid	Ter	All	Ini	Mid	Ter	All	Ini	Mid	Ter	All	Ini	Mid	Ter	All
-	Ave	-	-		-	-	-	-	-	-	-	-	-	-	-	0.2292	-	-	-	-	-	-	-	-	-	-	-	-	-	-	-	
-	Med	-	-		-	-	-	-	-	-	-	-	-	-	-	0.1702	-	-	-	-	-	-	-	-	-	-	-	-	-	-	-	
-	Q1st	-	-		-	-	-	-	-	-	-	-	-	-	-	-	-	-	-	-	-	-	-	-	-	-	-	-	-	-	-	
-	Q3rd	-	-		-	-	-	-	-	-	-	-	-	-	-	0.2311	-	-	-	-	-	-	-	-	-	-	-	-	-	-	-	
-	Var	-	-		-	-	-	-	-	-	-	-	-	-	-	-	-	-	-	-	-	-	-	-	-	-	-	0.226	-	-	-	
-	1 %ile	-	-		-	-	-	-	-	-	-	-	-	-	-	-	-	-	-	-	-	-	-	-	-	-	-	-	-	-	-	
-	5 %ile	-	-		-	-	-	-	-	-	-	-	-	-	-	-	-	-	-	-	-	-	-	-	-	-	-	-	-	-	-	
-	95 %ile	-	-		-	-	-	-	-	-	-	-	-	-	-	-	-	-	-	-	-	-	-	0.2395	-	-	-	-	-	-	-	
-	99 %ile	-	-		-	-	-	-	-	-	-	-	-	-	-	-	-	-	-	-	-	-	-	0.2316	-	-	-	-	-	-	-	
1	Ave	-	-	-				-				-				-				-				-				-				-
2	Ave	-	-	-				-				-				-				-				-				-				-
3	Ave	-	-	-				-				-				-		0.1464		-				-				-				-
3	Med	-	-	-				-				-				-				-	-	-	-	-				-				-
3	Var	-	-	-				-				-				-				-	-	-	-	-				-				-
4	Ave	-	-	-				-				-				-				-				-				-				-
4	Med	-	-	-				-				-				-				-	-	-	-	-				-				-
4	Var	-	-	-				-				-				-				-	-	-	-	-				-				-
5	Ave	-	-	-				-				-				-				-				-				-				-
5	Med	-	-	-				-				-				-				-	-	-	-	-				-				-
5	Var	-	-	-				-				-				-				-	-	-	-	-				-				-
6	Ave	-	-	-				-				-				-				-				-				-				-
6	Med	-	-	-				-				-				-				-	-	-	-	-				-				-
6	Var	-	-	-				-				-				-		0.1596		-	-	-	-	-				-				-

Supplementary Table 12. Statistical details of fly behavior with or without pheromone sensation.

Strain	Condition	Number of individuals	Parameter	Sample size	Size unit	Pre-test method	W	p.value	Adjusted p-value	Statistical method	Trial	W	p-value	Adjusted p-value	Significance
CS-H	with/without female tapping	27, 30	Speed	216, 240	frame	Shapiro-Wilk normality test followed by Bonferroni multiple comparisons	0.8332	1.74E-14	1.39E-13	Mann–Whitney U test followed by Bonferroni multiple comparisons	1	39850.5	1.32E-27	1.06E-26	***
							0.7979	5.16E-16	4.13E-15		2	39785	1.15E-29	9.17E-29	***
							0.6993	1.93E-19	1.55E-18		3	37212	1.18E-21	9.40E-21	***
							0.6949	1.43E-19	1.14E-18		4	36750.5	8.82E-21	7.06E-20	***
							0.6670	2.23E-20	1.79E-19		5	37393.5	6.19E-23	4.95E-22	***
							0.6246	1.65E-21	1.32E-20		6	35820	7.25E-20	5.80E-19	***
							0.5747	1.00E-22	8.04E-22		7	35069	2.42E-18	1.93E-17	***
							0.4664	5.07E-25	4.05E-24		8	32276.5	5.11E-11	4.09E-10	***

*: <0.05, **: <0.01, ***: <0.001

Supplementary Table 13. Statistical details of fly behavior over time.

Strain	Condition	Number of individuals	Parameter	Sample size	Size unit	Statistical method	Pairwise	t-value	p-value	Significance *: <0.05, **: <0.01, ***: <0.001
							Round1 - Round2	1.3909	0.8618	
							Round1 - Round3	2.6703	0.1317	
							Round1 - Round4	4.0959	0.0011	**
							Round1 - Round5	4.5992	0.0001	***
							Round1 - Round6	5.3908	0.0000	***
							Round1 - Round7	5.7592	0.0000	***
							Round1 - Round8	8.1549	0.0000	***
							Round2 - Round3	1.4020	0.8567	
							Round2 - Round4	2.7391	0.1110	
							Round2 - Round5	3.1492	0.0350	*
							Round2 - Round6	4.1184	0.0010	***
							Round2 - Round7	4.5341	0.0002	***
							Round2 - Round8	7.0061	0.0000	***
CS-H	with female tapping	27	Speed	216, 216	frame	Steel-Dwass test	Round3 - Round4	1.1840	0.9367	
							Round3 - Round5	1.4543	0.8316	
							Round3 - Round6	2.5448	0.1767	
							Round3 - Round7	2.9956	0.0554	
							Round3 - Round8	5.3568	0.0000	***
							Round4 - Round5	0.2134	1.0000	
							Round4 - Round6	1.5173	0.7984	
							Round4 - Round7	2.0747	0.4315	
							Round4 - Round8	4.5499	0.0001	***
							Round5 - Round6	1.4459	0.8357	
							Round5 - Round7	2.1206	0.4014	
							Round5 - Round8	4.6360	0.0001	***
							Round6 - Round7	0.5716	0.9992	
							Round6 - Round8	3.0009	0.0546	
							Round7 - Round8	2.3177	0.2837	
							Round1 - Round2	2.2918	0.2979	
							Round1 - Round3	2.2282	0.3346	
							Round1 - Round4	2.7780	0.1005	
							Round1 - Round5	3.1377	0.0363	*
							Round1 - Round6	4.1601	0.0008	***
							Round1 - Round7	4.6189	0.0001	***
							Round1 - Round8	4.4005	0.0003	***
							Round2 - Round3	0.0976	1.0000	
							Round2 - Round4	0.4862	0.9997	
							Round2 - Round5	0.9076	0.9854	
							Round2 - Round6	1.9230	0.5349	
							Round2 - Round7	2.3958	0.2432	
							Round2 - Round8	2.1949	0.3547	
CS-H	without female tapping	30	Speed	240, 240	frame	Steel-Dwass test	Round3 - Round4	0.5688	0.9992	
							Round3 - Round5	1.0209	0.9714	
							Round3 - Round6	2.0194	0.4685	
							Round3 - Round7	2.4846	0.2019	
							Round3 - Round8	2.2974	0.2949	
							Round4 - Round5	0.4170	0.9999	
							Round4 - Round6	1.4279	0.8445	
							Round4 - Round7	1.9115	0.5429	
							Round4 - Round8	1.6973	0.6891	
							Round5 - Round6	0.9956	0.9752	
							Round5 - Round7	1.4837	0.8165	
							Round5 - Round8	1.2886	0.9034	
							Round6 - Round7	0.5014	0.9997	
							Round6 - Round8	0.2959	1.0000	
							Round7 - Round8	0.2021	1.0000	

ACKNOWLEDGEMENT